Pitch and Roll Corrections for the CLARIFY-2017 Radiation Data

OBR Technical Note 91

23 July 2018

Anthony Jones, Jim Haywood, Alan Vance and Claire Ryder

Correspondence: anthony.jones@metoffice.gov.uk

If printing double sided you will need this blank page. If printing single sided, please delete this page.

Contents

1. Motivation

Pitch and roll (P&R) corrections are applied to aircraft radiation data in order to account for deviations to direct solar irradiance with attitude (i.e. an aircraft's deviation from the horizontal) [Saunders *et al*., 1992]. However, the P&R methodology is not well documented in recent literature and hence is rather esoteric, despite being simple to implement. The Facility for Airborne Atmospheric Measurements (FAAM) automatically apply P&R corrections to data from the Eppley Broad Band Radiometers (BBRs), with coefficients derived from previous campaigns, but in reality new P&R coefficients should be determined each time a sensor is removed and then reaffixed to the aircraft. Additionally, some radiation-measuring instruments aboard the FAAM aircraft are not included in the core set of data processed by FAAM (e.g. SHIMS), yet are still subject to the same P&R tendencies. Previous MRF and OBR reports have described attitude corrections in some detail [MRF internal notes 4, 31, 56; MRF technical notes 5, 8]. In addition, various historical papers have also described the method [e.g. Cluley and Cowley, 1980; Saunders *et al*., 1992; Bannehr and Schwiesow, 1992; Boers *et al*., 1998]. In this report, we re-document the P&R methodology and then apply P&R corrections to radiation data collected during the CLARIFY-2017 campaign, which flew from the Ascension Island in August/ September 2017.

2. Methodology

2.1 Pitch and roll correction overview

Adopting general convention, we let the pitch (P) denote the angle between the aircraft's longitudinal axis and the horizontal and the roll (R) denote the angle between the aircraft's transverse axis and the horizontal. P&R corrections also require information about the sun's position relative to the aircraft heading, i.e. the solar zenith angle (θ), the solar azimuthal angle (α), and the aircraft heading (H). The relative heading is then defined as $H_S = \alpha - H$, where $H_S = 0^o$ indicates that the aircraft is facing toward the sun. Finally, we require information on the direct to total irradiance (F_{DIR}) ratio and the cosine correction factor for the sensor (C_{eff}) [MRF Internal Note 31]. The aircraft does not directly measure F_{DIR}, therefore we pragmatically use an offline radiation code and a standard atmospheric profile to estimate F_{DIR} as a function of aircraft altitude (Z) and θ. F_{DIR} can only be estimated in such a way for clear-sky conditions, or without a significant amount of cloud or aerosol. C_{eff} is an instrument-dependent ratio that accounts for errors arising from inhomogeneity in the radiation field [Saunders *et al*., 1992]. C_{eff} optimally equals one for all θ (indicating a perfect cosine response), but in practice often decreases as θ increases. C_{eff} has been measured for the BBRs but not for the SHIMS (Spectral Hemispheric Irradiance Measurements) instrument, for which we pragmatically use the BBR values. The P&R correction is of the following form:

$$\cos\beta = (\sin R \times \sin\theta \times \sin H_s) + (\cos R \times \cos P \times \cos\theta) - (\cos R \times \sin P \times \sin\theta \times \cos H_s) \quad (2.1)$$

$$F_{\downarrow,cor}(\theta) = \frac{F_{\downarrow}(\theta)}{1 - F_{DIR} \times \left(1 - C_{\text{eff}} \times \frac{\cos\beta}{\cos\theta}\right)} \quad (2.2)$$

Pitch and roll deviations for the aircraft (*P'* and *R'*) are derived from the on-board GIN sensor, but the *P* and *R* values in Eq. 2.1 also require knowledge of how the sensors are fitted to the aircraft. *P* and *R* are thus decomposed: $P = \Delta P + P'$ and $R = \Delta R + R'$ where ΔP and ΔR are offsets resulting from imperfect fitting of the sensor to the aircraft. When the aircraft was commissioned, the BBRs were mounted at 3º to the horizontal, which suggests that a pitch offset of ΔP = -3º should be optimal. ΔR values from previous campaigns have typically been close to 0º, for instance ΔR = -0.4º in the GERBILS campaign [Haywood *et al*., 2011]. However, that campaign also used ΔP = +0.4º, which suggests that the ΔP = -3º and ΔR = 0º default values used by FAAM may not be optimal in all applications to FAAM data. Values for ΔP and ΔR are instrument dependent - optimal values may differ between flights and should be re-evaluated each time the instrument is refitted to the aircraft.

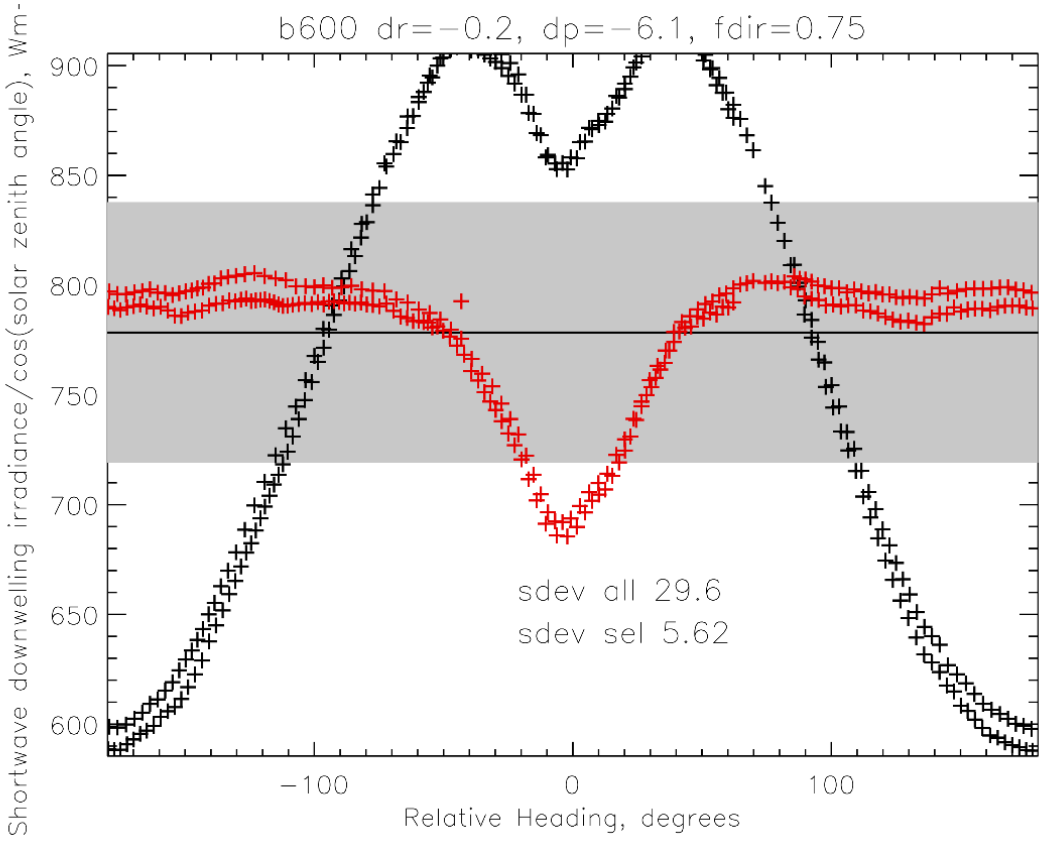

Figure 2.1: Normalized irradiances from a pirouette manoeuvre before flight b600 in the Fennec-2011 campaign [Ryder et al., 2013]. Black crosses are uncorrected irradiances and red crosses are pitch and roll corrected irradiances (Eqs 2.1-2.2)

2.2 Constraints on pitch and roll offsets and radiation data

Fitting P&R offsets to the radiation data is not straightforward. Firstly, only upward facing instruments need P&R corrections as downward facing instruments are subjected only to diffuse solar radiation, whereas the P&R corrections are a direct solar radiation issue. Secondly, it is often difficult to distinguish between direct and diffuse solar radiation and a threshold is usually applied above which radiation is assumed to be primarily direct and thus P&R corrections are necessary [Schmetz and Beniston, 1986].

$$F_{\text{crit}} = 920 \times (\cos\theta)^{1.28} \tag{2.3}$$

Thirdly, the instruments are susceptible to sandblasting and general contamination. Figure 2.1 shows normalized irradiances (i.e. divided by the cosine of θ) from a double pirouette manoeuvre performed before take-off on flight b600 in the Fennec-2011 campaign [Ryder *et al.*, 2013]. The black crosses in Fig. 2.1 show the uncorrected irradiances ($F_{\downarrow}(\theta)$ in Eq. 2.2) and the red crosses show the P&R corrected irradiances ($F_{\downarrow,cor}(\theta)$ in Eq. 2.2). Note that the P&R offsets are ΔP = -6.1º, ΔR = -0.2º, and a direct to total irradiance ratio of $F_{DIR} \equiv 0.75$ is used. The P&R correction has clearly equilibrated the normalized irradiances at large relative heading values ($|H_S| > 50$º), but there is an interesting trough signature at smaller $|H_S|$ values. This is consistent with damage to the front of the dome by regular sandblasting, with the affected region being less sensitive to direct solar radiation than the rest of the dome.

Another issue arises when the sun is at extremities, i.e. near directly above the aircraft or conversely, near the horizon. At low solar zenith angles (sun close to overhead) there is little deviation in irradiance with relative heading, while at high solar zenith angles (sun close to the horizon) irradiances are susceptible to tail shadowing when the aircraft is facing away from the sun (Fig. 2.2).

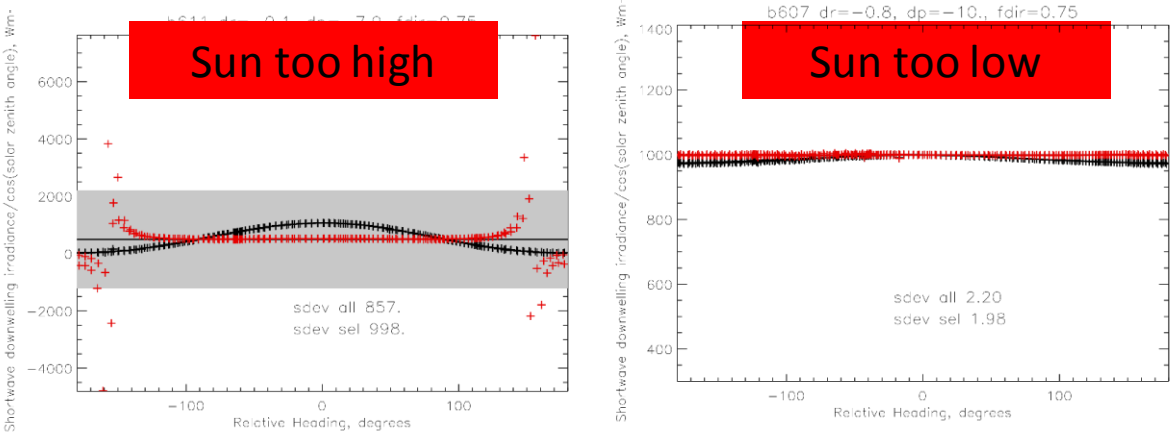

Figure 2.2: Example of periods when the sun was too high (left) and too low (right) to perform a reasonable pitch and roll correction. Data from pirouettes performed during the Fennec-2011 campaigns

Deriving P&R offsets (ΔP, ΔR) requires consideration of the issues listed above. Additionally, P&R offsets should be determined from targeted aircraft manoeuvres that record irradiances at a variety of relative headings spanning

$-180^o < H_s < 180^o$ whilst in clear-sky conditions. Targeted manoeuvres include L-shapes, box patterns (both performed at high altitudes to avoid cloud and tropospheric aerosol contamination) and pirouettes in clear sky conditions. Irradiance patterns from pirouettes should closely follow a cosine-like pattern such as seen in Fig. 2.1. Spurious deviances from this smooth cosine function may be unphysical or related to cloud contamination, and affected pirouette manoeuvres should be discarded when deriving ΔP and ΔR. Additionally, manoeuvres performed when θ is outside the range $15^o < \theta < 74^o$ should be ignored for the reasons highlighted in Fig. 2.2. At low solar zenith angles ($\theta < 15^o$) there is not much variation in solar irradiance with aircraft relative heading while at high solar zenith angles ($\theta > 74^o$), the total irradiance is low and tail shadowing can be a problem. These specific criteria were derived from the ICE-D and Fennec campaigns.

The aim of the P&R correction is to equilibrate irradiances for different relative headings and pitch and roll angles. Figure 2.3 shows examples of pitch-only and roll-only corrections from a pirouette manoeuvre. A negative pitch offset (Fig. 2.3 left) reduces or inverts the cosine shape of the irradiance distribution while a negative roll offset (Fig. 2.3 right) results in a right-shift in the irradiance distribution toward positive relative-headings. For this particular pirouette (Fig. 2.3), optimal P&R offsets that equilibrate the irradiances are $\Delta P = -2.8^o$ and $\Delta R = 0.4^o$, close to the standard FAAM values. Application of the P&R correction reduces the standard deviation of the irradiances to < 1 Wm^{-2} in this particular scenario. However, values for ΔP and ΔR may differ wildly between manoeuvres performed on the same campaign, for instance, on the ICE-D campaign, values for ΔP ranged from -6.8^o to -1.8^o, with a mean value of -4.6^o, while values for ΔR ranged from -0.3^o to $+4^o$, with a mean value of $+0.9^o$. Note that ΔP will change with aircraft weight, and so will reduce during any flight as fuel is burnt.

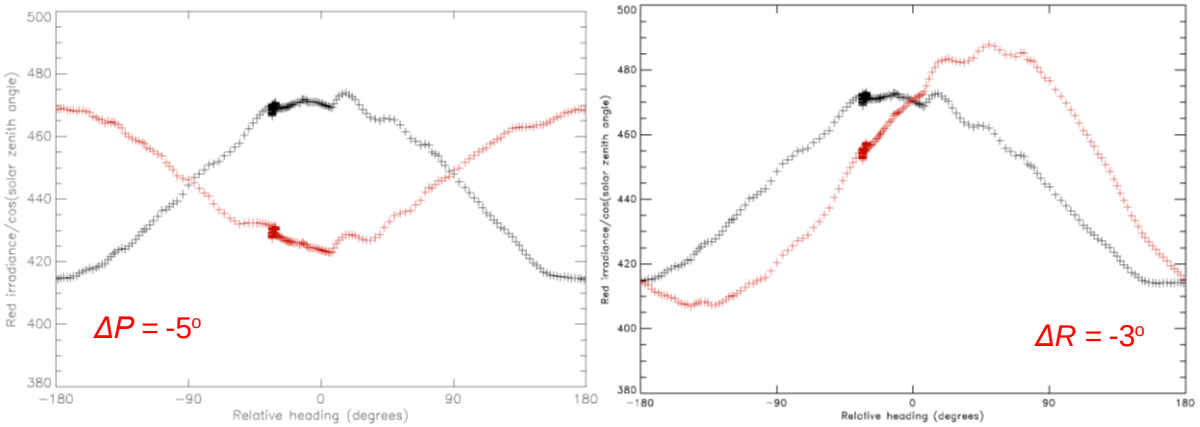

Figure 2.3: Examples of irradiance corrections for pitch only (left) and roll only (right). Black crosses represent raw irradiances and red crosses represent corrected irradiances. Data is from the Eppley red-dome BBR during a pirouette conducted at Cranfield (UK)

2.3 Optimization procedure for pitch and roll offsets

Calculating ΔP and ΔR coefficients is a numerical optimization problem with many possible algorithms available. Ultimately, the aim of the optimization is to find values of ΔP and ΔR that minimize the standard deviation of the normalized corrected irradiances ($F_{\downarrow,cor}(\theta)$/ cos θ). Bannehr and Schwiesow (1992) describe the skeleton of such an algorithm, which comprises the following steps. Note, that the algorithm begins with $\Delta P = \Delta R = 0$.

1. Calculate the corrected fluxes for the given values of θ, H_S, F_{DIR}, C_{eff}, P (= $\Delta P + P'$) and R (= $\Delta R + R'$) using Eqs 2.1 and 2.2. Note that ΔP and ΔR are held constant for each iteration of this algorithm; θ, H_S, P', and R' are from the aircraft, whilst F_{DIR} and C_{eff} must be approximated.

2. Perform a low-pass filter (either using quadratic fit, a constant function of cos θ, or some fitted irradiances as a function of θ and Z from a standard atmosphere + radiation code) to determine any trends caused by changing solar altitude

3. Subtract the low-pass filtered time series from the unfiltered time-series to obtain a series of high frequency residuals with zero mean. Else obtain the residuals from $F_{\downarrow,cor}(\theta)$/ cos θ for expediency

4. Determine the standard deviation (σ) of the residual time series. The ΔP angle is found by searching iteratively for the minimum standard deviation of the residual time series while ΔR is held constant

5. Using the retrieved ΔP as a new input parameter, a better estimate of ΔR is then determined iteratively. Repeat 1-5 until $|\Delta P_n - \Delta P_{n-1}|$ and $|\Delta R_n - \Delta R_{n-1}|$ (where n is the iteration number) are less than 0.001^o

Steps 4 and 5 require a suitable optimization algorithm. For example, we use a very simple golden section search that comprises the following steps for the specific example of optimizing ΔR. The algorithm begins with initial boundaries $\Delta R^1 = -90^o$ and $\Delta R^2 = +90^o$ and ends when $|\Delta R^2 - \Delta R^1| \leq 10^{-3\,o}$ at which point ΔR is set to the midpoint of ΔR^1 and ΔR^2. This simple algorithm takes approximately 25 iterations to converge. The algorithm uses a constant: $c = (-1 + \sqrt{5}) / 2$. We begin by evaluating the standard deviations of the corrected fluxes normalized by cos (θ) on 2^o ΔR increments from -90^o to 90^o in order to find a 4^o interval containing the global minima (it was found that many local minima existed between -90^o to 90^o). In this way, the golden section search offers more of a refinement than a true optimization tool.

1. Define $x^1 = c \times \Delta R^1 + (1 - c) \times \Delta R^2$ and $x^2 = (1 - c) \times \Delta R^1 + c \times \Delta R^2$. Calculate the corrected fluxes using x^1 and x^2 as roll offsets in Eqs 2.1 and 2.2, and then determine the standard deviations of the corrected fluxes normalized by cos (θ). Note that measurements conducted when $-40^o < \theta < 40^o$ are ignored when calculating the standard deviations. Denote the standard deviations σ^1 and σ^2 respectively

2. If ($\sigma^1 < \sigma^2$) then set $\Delta R^2 = x^2$, $x^2 = x^1$, $\sigma^2 = \sigma^1$, $x^1 = c \times \Delta R^1 + (1 - c) \times \Delta R^2$ and determine a new value of σ^1 using Eqs 2.1 and 2.2. Repeat step 2 if $|\Delta R^2 - \Delta R^1| > 10^{-3}$ o

3. Else set $\Delta R^1 = x^1$, $x^1 = x^2$, $\sigma^1 = \sigma^2$, $x^2 = (1 - c) \times \Delta R^1 + c \times \Delta R^2$ and determine a new value of σ^2 using Eqs 2.1 and 2.2. Return to step 2 if $|\Delta R^2 - \Delta R^1| > 10^{-3}$ o

The above algorithm requires estimates for F_{DIR} and C_{eff} (Eq. 2.2). C_{eff} as measured for the BBRs is shown in Fig. 2.4 and varies between 1.01 for overhead sun to 0.93 for low solar altitudes. F_{DIR} will depend on the atmospheric conditions, the altitude surveyed, and more importantly, the wavelength spectrum under consideration. Approximate boundaries for the wavelength spectra of the instruments studied here are provided in Table 2.1. Subtracting the irradiances from the BBR red dome from the BBR clear dome provides a short-wave spectrum spanning 0.3-0.7 µm that is comparable to the equivalent wavebands from the SHIMS visible module. This comparison is not perfect as neither the response of the BBR thermopiles nor the transmission of the dome glasses are mathematical boxcars. Instead, one should calculate an effective transfer function and convolve the SHIMS data with this, rather than simply summing SHIMS pixels [see OBR Technical Note 90].

Instrument	Min Wavelength (µm)	Max Wavelength (µm)	Increment (µm)
BBR clear dome	0.3	3	-
BBR red dome	0.7	3	-
SHIMS visible	0.303	1.15	0.0033
SHIMS near-infrared	0.948	1.69	0.0033

Table 2.1: Wavelength spectra details for the various instruments/ modules. Note that for SHIMS, pixel widths are not uniform and may vary by ±5 % for both modules

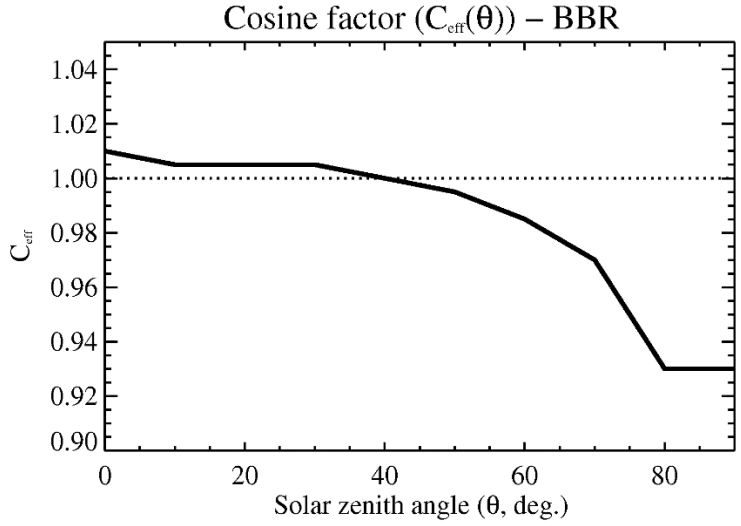

Figure 2.4: Cosine factor as a function of solar zenith angle for the BBRs

We now approximate F_{DIR} as a function of solar zenith angle and altitude using the SOCRATES radiation code [Edwards and Slingo, 1996], and a single-column cloud-free atmosphere representing standard tropical conditions [McClatchey *et al*., 1972; Jones, 2017]. We also include a stratospheric sulphate layer with mass mixing ratios derived from a present day simulation with HadGEM3-A, which has a 0.55 μm optical depth of ~0.0125. A spectral file with 220 wavebands in the short-wave spectrum (0.2 – 10 μm) is used, with the relevant wavebands extracted for each instrument (Table 2.1). F_{DIR} is determined from the ratio of the downwelling direct solar flux to the total downwelling radiative flux, using 5° θ increments and 0.5 km altitude increments from the surface to 10 km altitude.

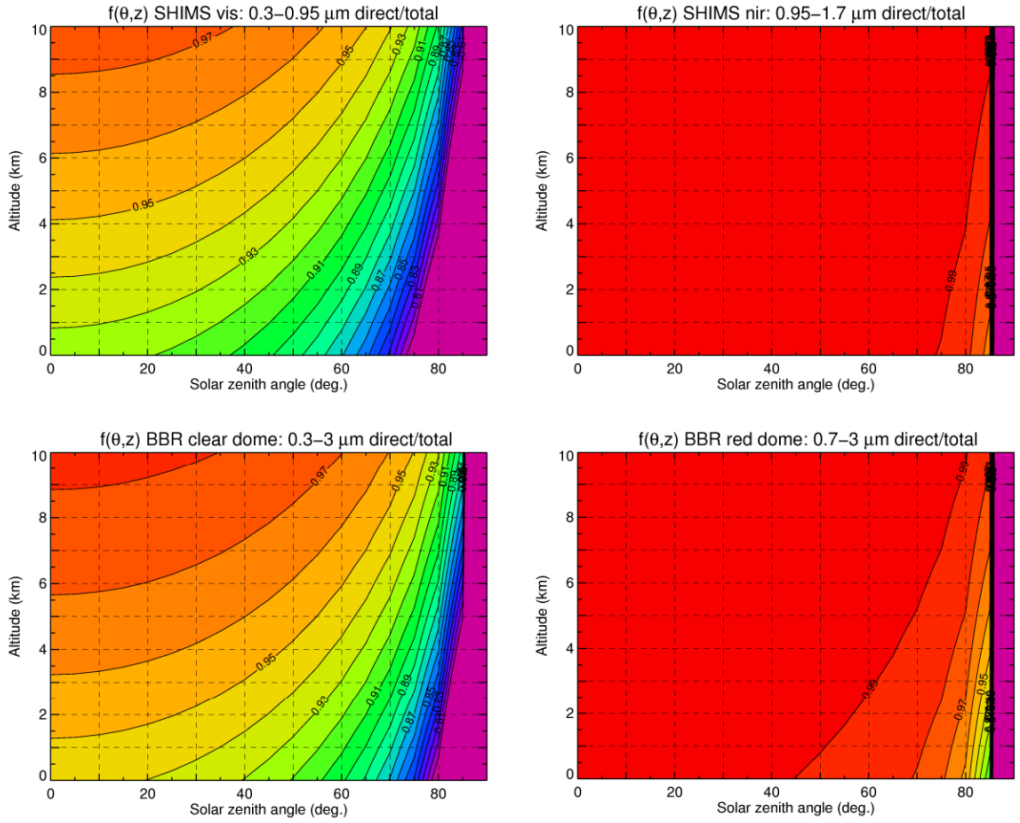

Figure 2.5: Ratio of direct to total downwelling SW flux as a function of solar zenith angle and altitude

Figure 2.5 shows resulting F_{DIR} values as a function of solar zenith angle and altitude. F_{DIR} for the visible modules (SHIMS vis and BBR clear) is approximately equal to 0.95 at 6 km altitude and θ = 45° which agrees with FAAM's recommended F_{DIR} estimate for high-altitude box patterns. However, there will be significant altitude and θ dependence as the instruments survey different wavelengths (Table 2.1) and Rayleigh scattering is strongly wavelength dependent over the visible spectrum. Only at the surface and at very high solar zenith angles (θ > 80°) does F_{DIR} reach 0.75 for the wavebands corresponding to BBR clear and SHIMS vis, as assumed in Figs 2.1-2.2. The BBR red dome and SHIMS near-infrared module show weak dependence of F_{DIR} on altitude and θ suggesting that a uniform approximation of ~0.99 should suffice in clear-sky conditions. Note that the two SHIMS modules will have the same attitude (ΔP, ΔR) dependence as they use the same receiver. Light is collected in a fibre

bundle which transmits it to the rack, where the bundle splits, to go to the two detector modules (visible and near-infrared).

2.4 Inverting FAAM's corrections

Before proceeding to the results section, it is important to note that FAAM often apply their own P&R corrections to the BBR data as stored in the processed core files on the CEDA data server (http://data.ceda.ac.uk). The filenames indicate whether such processing has been performed, for instance v004 in the following file name indicates P&R processing: core_faam_20170828_*v004*_r0_c043.nc. The metadata in this file also gives the P&R offset values that used in the correction:

```
"pitch and roll offsets changed post FENNEC pilot campaign after a
recommendation from Claire Ryder, who analysed the pirouette and the box
pattern from flight B597 27/05/2011",
"rflux   Corrected BBR fluxes - TA,TB,TC,Pit,Rol,Obs (1=none 2=small
3=large)",
"CALCUCF   0.00000E-3  0.00000E+0  0.00000E+0 -2.80000E+0  0.30000E+0
1.00000E+0",
"CALCURF   0.00000E-3  0.00000E+0  0.00000E+0 -3.20000E+0 -0.10000E+0
1.00000E+0",
```

In this case, the P&R offsets for the upper BBR clear dome (CALCUCF) were -2.8º and +0.3 º respectively, and for the upper BBR red dome (CALCURF) were -3.2 º and -0.1º respectively. The post processing procedure that FAAM uses is C_RFLUX.fort (http://decades-pp.readthedocs.io/en/latest/fortran_modules.html). FAAM applies P&R corrections if the following criteria are met:

- The absolute value of the corrected roll angle ($R = \Delta R + R'$) is less than 7º
- The solar elevation angle β (Eq. 2.1) is less than 80º
- The flux is greater than F_{crit} (Eq. 2.3) for the clear dome or greater than 0.5 × F_{crit} for the red dome

Additionally, the P&R measurements (P', R') that FAAM uses are the average of the values from the 2 preceding seconds from the General Inertial Navigation (GIN) unit and F_{DIR} is prescribed as 0.95. We now aim to invert the FAAM P&R correction to obtain raw irradiance measurements for the BBRs. As an example of the inversion process, we use data from the first leg of a box pattern on CLARIFY flight C028 (16/08/2017). The following values are time-averages: θ = 29.6º, φ = 44.7º, H = 49º, $F_{\downarrow}$ = 1045 Wm^{-2}, P' = 5.7º, R' = -0.5º. Here, $F_{\downarrow}$ denotes the FAAM corrected irradiance from the upper BBR clear dome. We also assume F_{DIR} = 0.95 and C_{eff} = 1.005. The pitch and roll values are then $P = \Delta P + P'$ = 5.7º - 2.8º = 2.9º and $R = \Delta R + R'$ = -0.5º + 0.3º = -0.2º. The inverted or raw irradiance value is then determined to be 1020 Wm^{-2} using the following equation.

$$F_{\downarrow,uncor} = F_{\downarrow} \times \left[1 - F_{DIR} \times \left(1 - C_{\text{eff}} \times \frac{\cos\beta}{\cos\theta}\right)\right] \qquad (2.4)$$

Flight	Manoeuvre	Date / Start time / End time	Average Solar Zenith Angle (θ, deg.)	$15^o < \theta < 74^o$
C028	Pirouette (start)	16/08/2017 08:49:04 08:51:22	66	Yes
C028	Box	16/08/2017 11:33:18 12:19:44	26-31	Yes
C029	Pirouette (end)	17/08/2017 12:35:11 12:36:58	22	Yes
C030	Pirouette (end)	17/08/2017 17:52:31 17:54:03	75	No
C032	Pirouette (start)	19/08/2017 09:54:45 09:55:57	50	Yes
C037	Pirouette (end)	24/08/2017 17:00:05 17:01:36	63	Yes
C038	Pirouette (start)	25/08/2017 08:54:03 08:56:03	64	Yes
C040	Pirouette (start)	26/08/2017 08:48:59 08:50:22	65	Yes
C043	Box	28/08/2017 16:25:22 16:44:27	55-59	Yes
C052	Pirouette (end)	05/09/2017 17:46:37 17:48:28	74	No

Table 3.1: Attitude manoeuvres and times during the CLARIFY-2017 campaign

3. Deriving pitch and roll offsets for CLARIFY-2017

As with previous campaigns, various pirouette and box pattern manoeuvres were performed during CLARIFY-2017. Table 3.1 lists these manoeuvres and relevant temporal details. Two of the pirouettes (C030 and C052) were performed when the solar zenith angle exceeded 74^o indicating that aircraft tail shadowing may be present in these cases and data should be treated with caution Only two box patterns were performed during CLARIFY (C028 and C043), both at an altitude of approximately 6 km and both with 4 legs.

3.1 BBR Clear Dome

In previous campaigns with the FAAM aircraft, data collected when the relative heading was less than ±50º was ignored when applying P&R corrections due to sandblasting and contamination at the front of the dome affecting irradiances at small relative headings (e.g Fig. 2.1). For this this campaign, it was decided that ±40º rather than ±50º would be a better threshold as two of the legs of the box pattern in C043 were performed when the relative heading was between ±40º and ±50º and hence the new ±40º threshold would not exclude either leg. There is clear evidence of contamination at small relative headings in the post-flight pirouette manoeuvres (C037, C052) in Fig. 3.1, validating our choice to ignore data at small relative headings. The dirty dip signature (i.e. the reduction in recorded irradiances at small solar zenith angles due to contamination on the dome) in these pirouettes is mostly confined to relative headings of ±40º, although the dip is not perfectly symmetrical about 0º and the lower threshold may therefore be suspect. The asymmetry about 0º may be due to the receivers being mounted slightly off-centre, and the hence airflow may not be axial about the receivers. Nevertheless, our choice of ±40º rather than ±50º as the threshold for this campaign should not affect results too much as the dirt dips are almost entirely confined to ±40º (Fig. 3.1).

Figure 3.1 shows the results of the inversion algorithm (Eq. 2.4) applied to the BBR clear dome irradiances for the box patterns and pirouette manoeuvres in CLARIFY. The FAAM corrections of ΔP = -2.9º and ΔR = +0.3º appear to do a reasonable job at equilibrating the data values for the box patterns (top 2 plots), and for the pirouettes: C037, C038, and C040. Many of the inverted irradiances (blue crosses in Fig. 3.1) exhibit unphysical data or deviations from a cosine signal, for instance, in much of C028 PIR, C030, and C032 PIR. The C029 pirouette, which was performed at approximately solar noon, is not equilibrated by FAAM's corrections, which suggests that the cosine correction factor C_{eff} may not be correct for this instrument and should be re-evaluated (Fig. 2.4).

Figure 3.2 shows the results of performing P&R optimizations on the inverted BBR clear dome irradiances, where optimal P&R coefficients are derived separately for each manoeuvre. The ΔP and ΔR coefficients are similar between the manoeuvres C043 BOX, C037, C038, C040, and C052 with $\Delta P \in$ [-2.4, -3.2] and $\Delta R \in$ [-0.6, +0.7]. In contrast, the C028 BOX and C029 manoeuvres have slightly larger pitch values of -4.6 and -5 respectively. From these results, we choose values $\boldsymbol{\Delta P = -3.2^o}$ and $\boldsymbol{\Delta R = 0^o}$ for the BBR clear dome, which will be applied to all of the CLARIFY data. Figure 3.3 shows that these values do a reasonable job at equilibrating irradiances for C043 BOX, C037 and C038. From the corrected irradiances (Fig. 3.3) we can approximate an error or uncertainty for the data collected from the instrument. Table 3.2 shows the 2σ uncertainty of the corrected irradiances as a percentage of the observed values. Only four manoeuvres demonstrated an acceptable P&R correction for BBR clear (C028 BOX, C037 PIR, C038 PIR, C043 BOX). From these manoeuvres, the 2σ uncertainty *due to P&R, dirt/damage, and cosine issues* ranges from **±1** to **±7 %,** with the larger value appropriate for low and high solar altitudes. Note however that this is additional uncertainty on top of the *instrumental* uncertainty, which we do not attempt to calculate here.

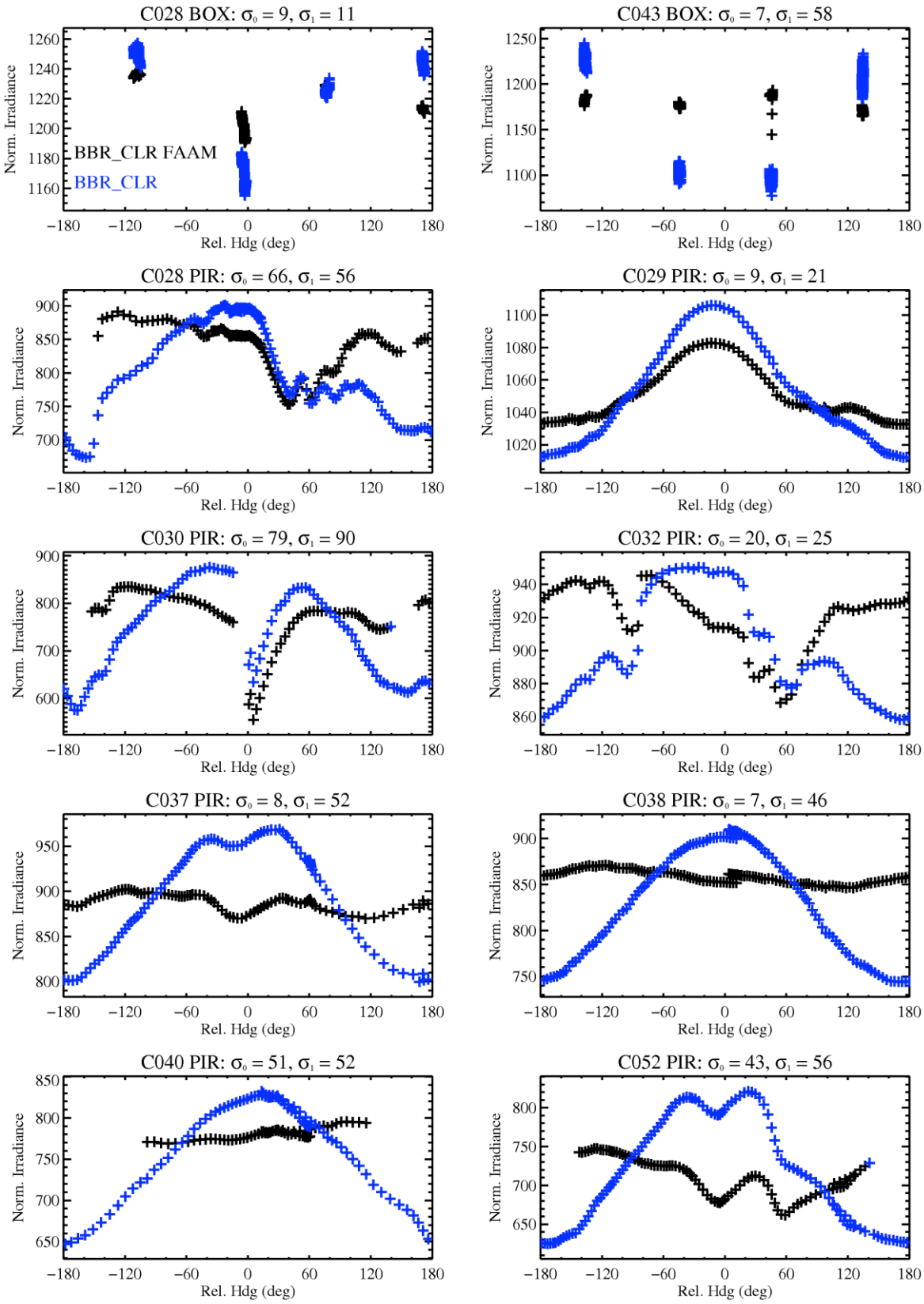

Figure 3.1: Normalised irradiances from the BBR clear dome for manoeuvres during the CLARIFY-2017 campaign. Black indicates data corrected by FAAM (ΔP = -2.8 º, ΔR = +0.3º), blue indicates data with corrections removed and values for FAAM and corrected standard deviations σ0 and σ1 are given in the titles

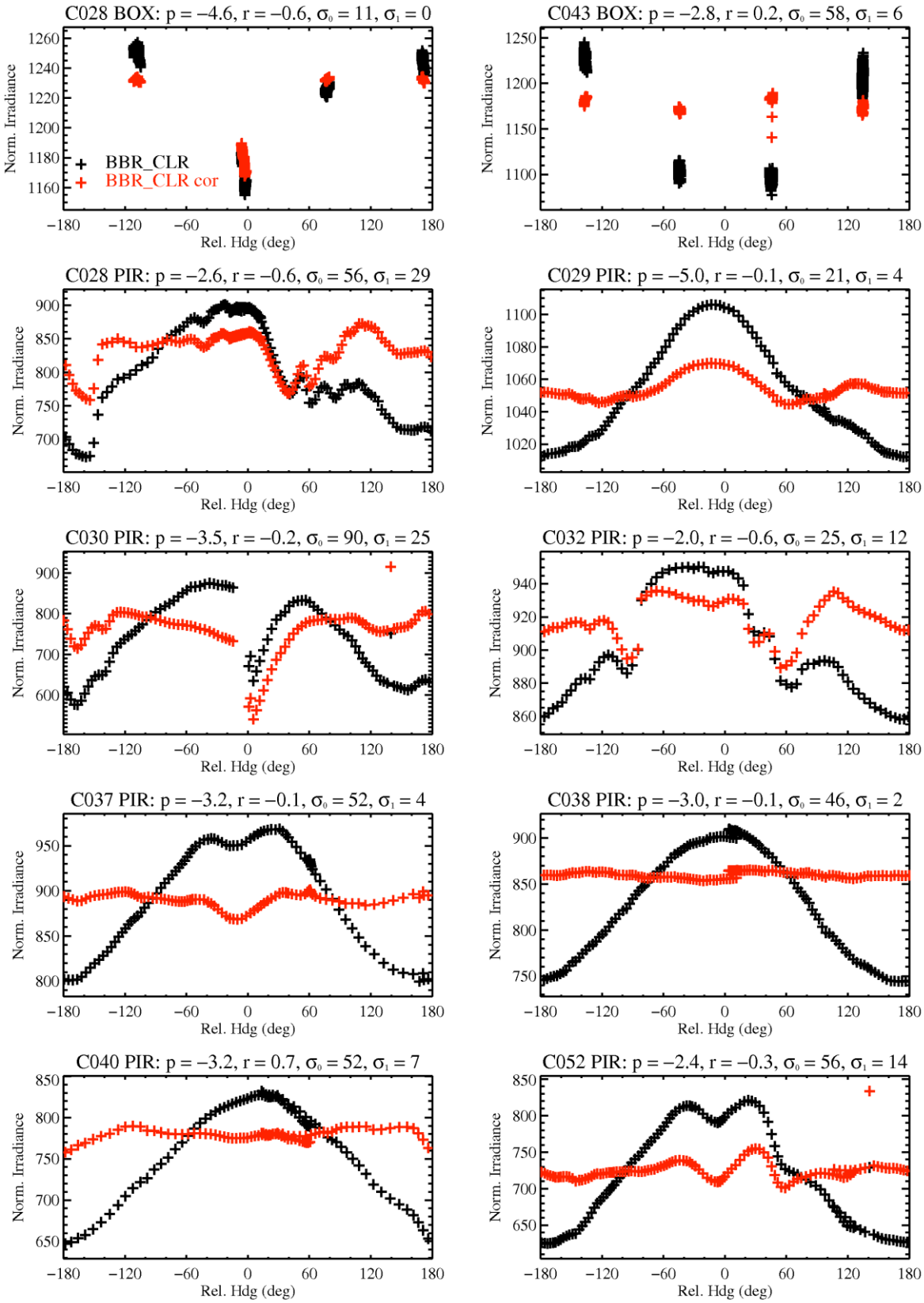

Figure 3.2: Normalised irradiances from the BBR clear dome for manoeuvres during the CLARIFY-2017 campaign. Black indicates raw data, red indicates data corrected by optimal attitude corrections (values for ΔP and ΔR are given in the titles, as well as initial and corrected standard deviations σ_0 and σ_1)

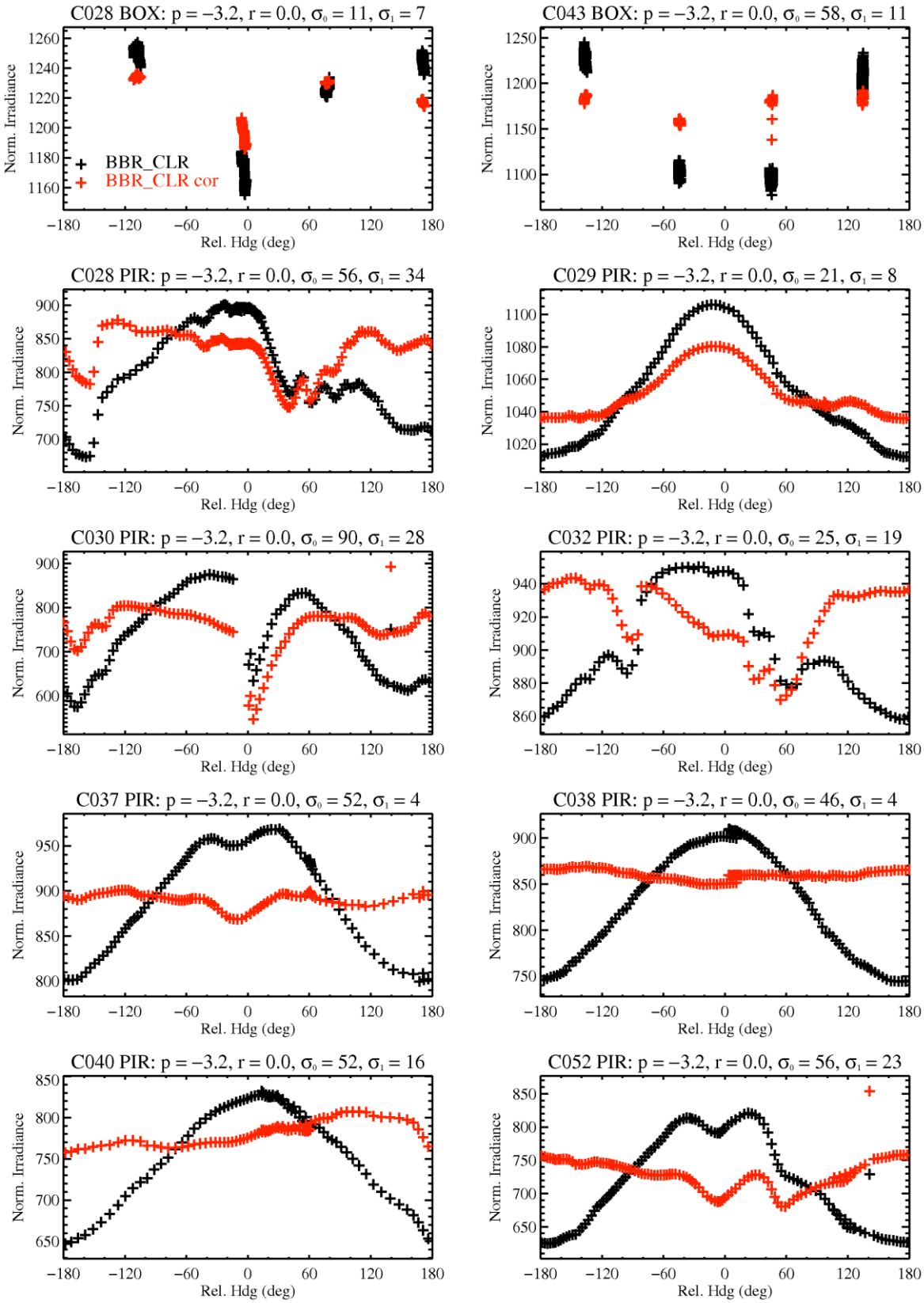

Figure 3.3: Normalised irradiances from the BBR clear dome for manoeuvres during the CLARIFY-2017 campaign. Black indicates raw data, red indicates data corrected by optimal attitude corrections of ΔP = -3.2 and ΔR = 0 (values for the initial and corrected standard deviations σ_0 and σ_1 given in the titles)

	2 × standard error of corrected irradiances as a percentage of total irradiance (%)			
Manoeuvre	BBR clear	BBR red	SHIMS visible	SHIMS near-infrared
C028 PIR	8.2 unphysical	17.4 unphysical	1.8 OK	2.9 OK
C028 BOX	1.2 OK	0.9 OK	4.6 θ too low?	5.3 θ too low?
C029 PIR	1.6 θ too low?	0.7 OK	5 θ too low?	5.7 θ too low?
C030 PIR	7.3 unphysical	10.5 unphysical	4.8 θ too big?	7.6 θ too big?
C032 PIR	4.3 unphysical	11.7 unphysical	2 OK	2.3 OK
C037 PIR	1 OK	11.7 unphysical	1 OK	2.3 OK
C038 PIR	1 OK	17.8 unphysical	2.2 OK	2.3 OK
C040 PIR	4.1 unphysical	7.2 unphysical	3.9 unphysical	5.8 unphysical
C043 BOX	1.9 OK	24.9 unphysical	1.3 OK	2.1 OK
C052 PIR	6.4 θ too big?	12.1 θ too big?	6.6 θ too big?	8.3 θ too big?
Range of OK/physical results	1 – 7 %	1 – 12 %	1 – 7 %	2 – 8 %

Table 3.2: Table showing twice the standard error of the corrected irradiances as a percentage of total irradiance for each manoeuvre and instrument. Manoeuvres that are deemed ok are marked as such, while reasons for rejecting manoeuvres are also provided.

3.2 BBR Red Dome

As with the BBR clear dome, FAAM applies standard P&R corrections to the BBR red dome data using ΔP = -3.2º and ΔR = -0.1º. These values were derived from P&R optimizations conducted during the Fennec-2011 and ICE-D campaigns. Therefore, we invert the irradiances using Eq. 2.4 before any further P&R optimizations are performed. Figure 3.4 shows the results of the inversion process, with FAAM corrected values in black and the inverted values in blue. It is clear that only one pirouette exhibits a reasonable cosine irradiance pattern (C029); the other pirouettes, with the possible exceptions of C037 and C040 mostly exhibit unphysical patterns. The FAAM corrections are not effective at equilibrating irradiances for C043 BOX either, although the C028 BOX exhibits a far better correction.

Figure 3.5 shows the results of applying P&R optimization to the inverted BBR red data. We focus on the manoeuvres C028 BOX, C029 PIR, and C040 PIR which provide the best equilibrations, and in which ΔP = [-2.2, -3.3, -3.7] and ΔR = [+0.9, +0.4, -0.5]. Informed by these manoeuvres, we chose values $\boldsymbol{\Delta P = -3.1^{o}}$ and $\boldsymbol{\Delta R = +0.3^{o}}$ for the BBR red dome, which we again apply to all of the CLARIFY data. Figure 3.6 shows the results of applying these values to the BBR red data for the pirouettes and box patterns. It is clear that these corrections are appropriate for the manoeuvres C028 BOX, C029 PIR, and C040 PIR, but make little positive impact for the rather noisy irradiances from the other manoeuvres. Unphysical data, such as prevalent in most of the BBR red manoeuvres (Fig. 3.6) may arise from cloud or other atmospheric influences or from contamination on the dome itself. As the irradiance patterns from the BBR clear dome (and SHIMS) are mostly cosine-like for the pirouettes, this suggests that the problem is not cloud contamination but the instrument itself. From the acceptable manoeuvres (C028 BOX and C029 PIR), we determine a 2σ uncertainty *due to P&R, dirt/damage, and cosine issues* range of **±1** to **±12 %**, with the larger uncertainty appropriate for low and high solar altitudes (Table 3.2). However, we add the caveat that only two out of the ten manoeuvres provided good quality data. We therefore highlight the importance of checking the dome casings for damage or contamination before future flights, and we recommend that data collected from the red-dome instrument be treated with caution. FAAM have retrospectively checked the red dome casing used for CLARIFY-2017 campaign and found no obvious damage that can explain the curious irradiance signatures in Fig. 3.6, suggesting a possible issue with the instrument itself.

3.3 SHIMS visible module

SHIMS is not a core instrument and so SHIMS data is not subject to the same automatic post-processing FAAM routines as the BBRs. Figure 3.7 shows the results of applying P&R optimizations to the SHIMS visible data from the CLARIFY pirouette and box manoeuvres. It is clear that all of pirouettes exhibit cosine-like irradiance patterns, with a few minor unphysical responses at -90º in C032 and +60º in C052. What is also clear is that C028 BOX and C029, which were performed at high solar altitudes (Table 3.1), exhibit anomalously large optimal pitch values of -7.8º and -9.1º respectively, while C030 and C052, which

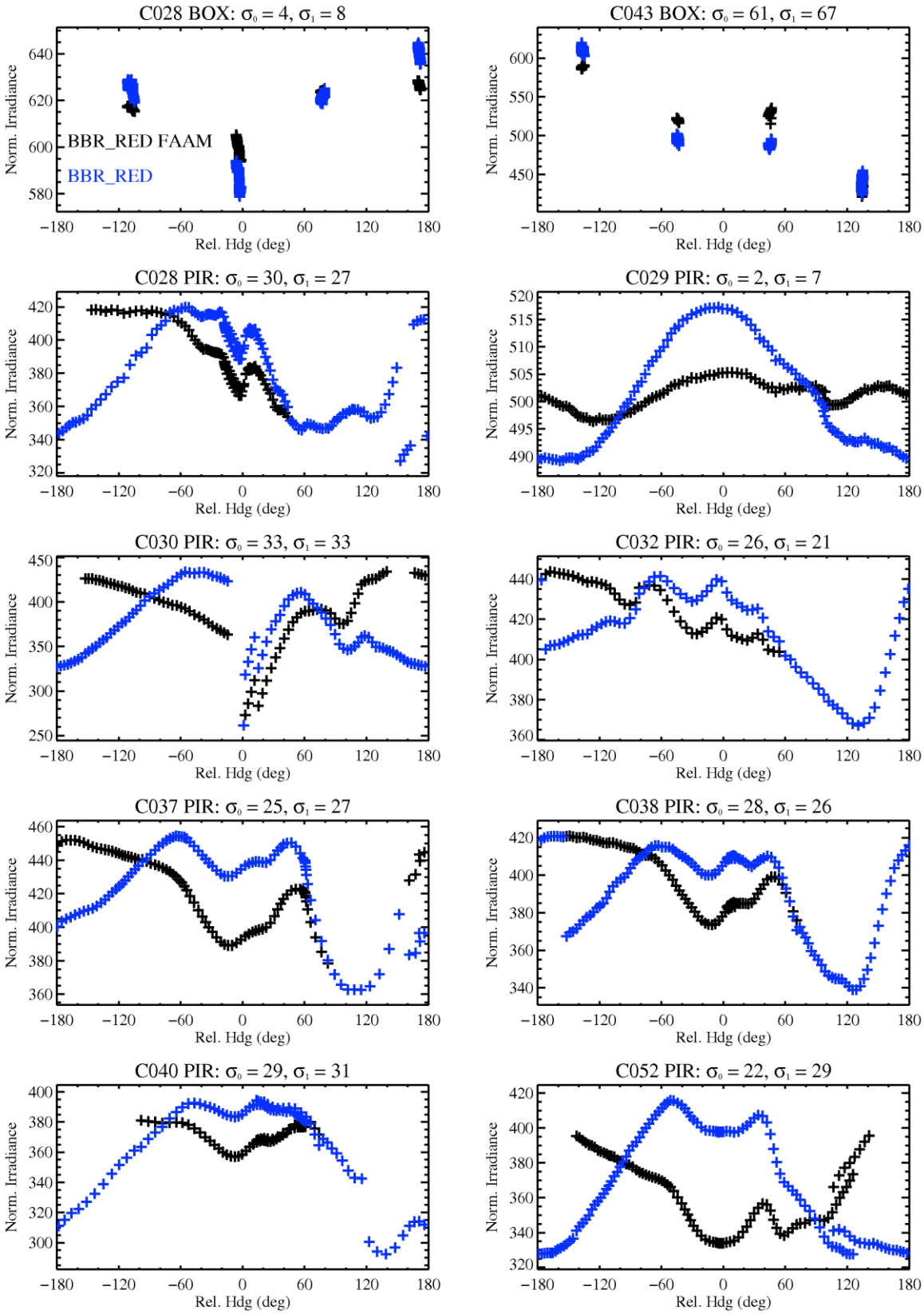

Figure 3.4: Normalised irradiances from the BBR red dome for manoeuvres during the CLARIFY-2017 campaign. Black indicates data corrected by FAAM (ΔP = -3.2 º, ΔR = -0.1º), blue indicates data with corrections removed and values for FAAM and corrected standard deviations σ_0 and σ_1 are given in the titles

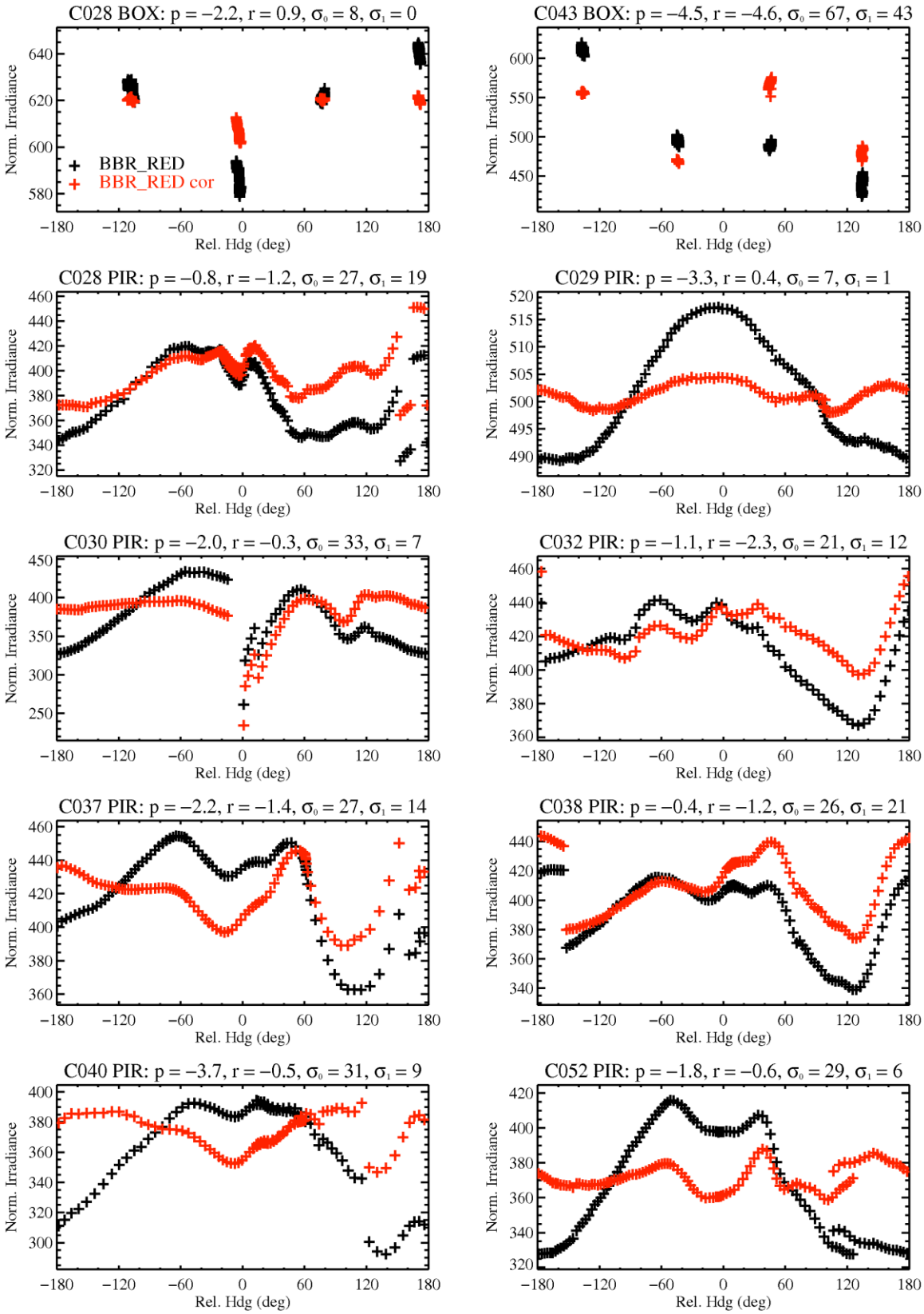

Figure 3.5: Normalised irradiances from the BBR red dome for manoeuvres during the CLARIFY-2017 campaign. Black indicates raw data, red indicates data corrected by optimal attitude corrections (values for ΔP and ΔR are given in the titles, as well as initial and corrected standard deviations σ_0 and σ_1)

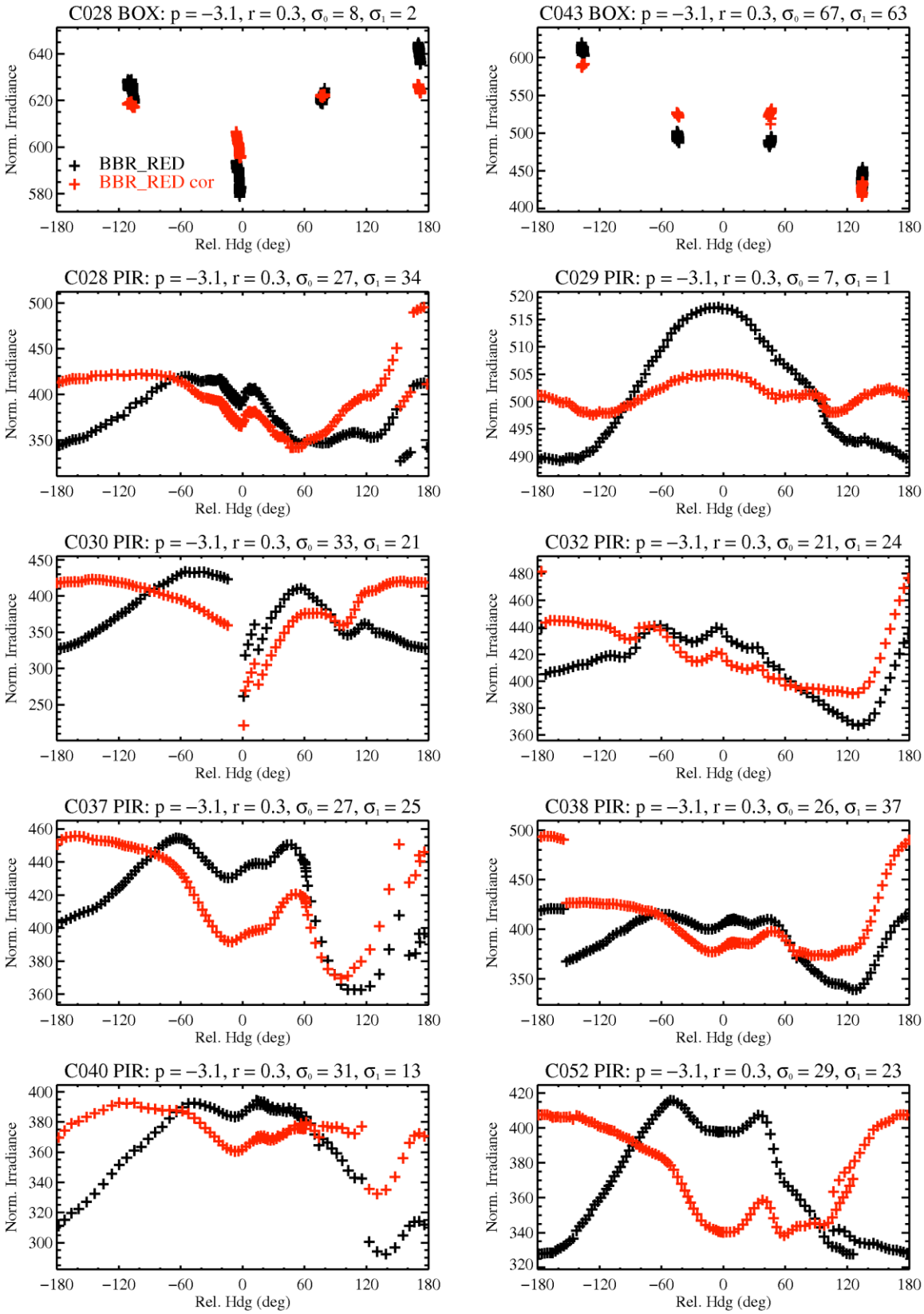

Figure 3.6: Normalised irradiances from the BBR red dome for manoeuvres during the CLARIFY-2017 campaign. Black indicates raw data, red indicates data corrected by optimal attitude corrections of ΔP = -3.1 and ΔR = +0.3 (values for the initial and corrected standard deviations σ_0 and σ_1 given in the titles)

were performed at low solar altitudes, exhibit small pitch values of -2.3º and -1.8º respectively. This suggests that the BBR-specific cosine correction factor (C_{eff}) utilized here may not be appropriate for SHIMS. This result is logical given that the BBRs are rotationally symmetric while the SHIMS receiver has a conical baffle and support, which gives the SHIMS' throughput an azimuthal dependence. In addition, the performance of the SHIMS' integrating sphere is unlikely to be perfect, which would mean that the throughput of the receiver could have a zenith angle dependence in addition to the aforementioned cosine response. Both of these dependencies need to be tested in order to fully calibrate the SHIMS measurements.

Using the P&R results of the manoeuvres and by optimizing data from the near-infrared module (which will necessarily have the same attitude dependence), we have chosen to utilise P&R values of $\boldsymbol{\Delta P = -3^o}$ and $\boldsymbol{\Delta R = +0.3^o}$ for the SHIMS visible module for the entirety of the campaign. Figure 3.8 shows the results of applying these P&R values to the manoeuvres. Normalized irradiances are effectively equilibrated for C043 BOX, C028 PIR, C032, C037, C038 and C040 (to less than 4 Wm^{-2}) giving us confidence in these P&R offsets. From the successful manoeuvres (Table 3.2), we find a 2σ uncertainty *due to P&R, dirt/damage, and cosine issues* of **±1** to **±7 %**, where the larger value is derived from the manoeuvres performed at low or high solar altitudes. A recent OBR tech note using laboratory measurements finds *instrumental* uncertainties of ±7 to ±10 % for the SHIMS instrument, which is on top of the uncertainty due to P&R, dirt/damage, and cosine issues [OBR Technical Note 90].

3.4 SHIMS near-infrared module

Figure 3.9 shows the raw normalized irradiances and optimized P&R corrected values for the SHIMS near-infrared module for each manoeuvre. Clearly, all of the pirouettes exhibit a cosine-like signal that peaks at relative heading ≅ 0º. Again, we see that C028 BOX and C029 PIR have anomalously large optimal pitch values, while C030 and C052 have anomalously small pitch values indicating that BBR C_{eff} values may not be appropriate for SHIMs. The optimal pitch values from the rest of the manoeuvres vary from -2.6º to -3.5º and the roll varies from 0.1º to 1º. Differences in optimal attitude corrections between the SHIMS visible and near-infrared modules are small (as expected) as the two modules use the same receiver. In keeping with our results from the SHIMS visible module, we therefore choose P&R offsets of $\boldsymbol{\Delta P = -3^o}$ and $\boldsymbol{\Delta R = +0.3^o}$ to be applied to all of the SHIMS near-infrared data. Figure 3.10 confirms that these values are generally appropriate by the fact that most of the normalized irradiances are effectively equilibrated. From the successful manoeuvres (Table 3.2), we determine a 2σ uncertainty *due to P&R, dirt/damage, and cosine issues* ranging from **±2** to **±8 %**, where the larger value is derived from the manoeuvres performed at low or high solar altitudes.

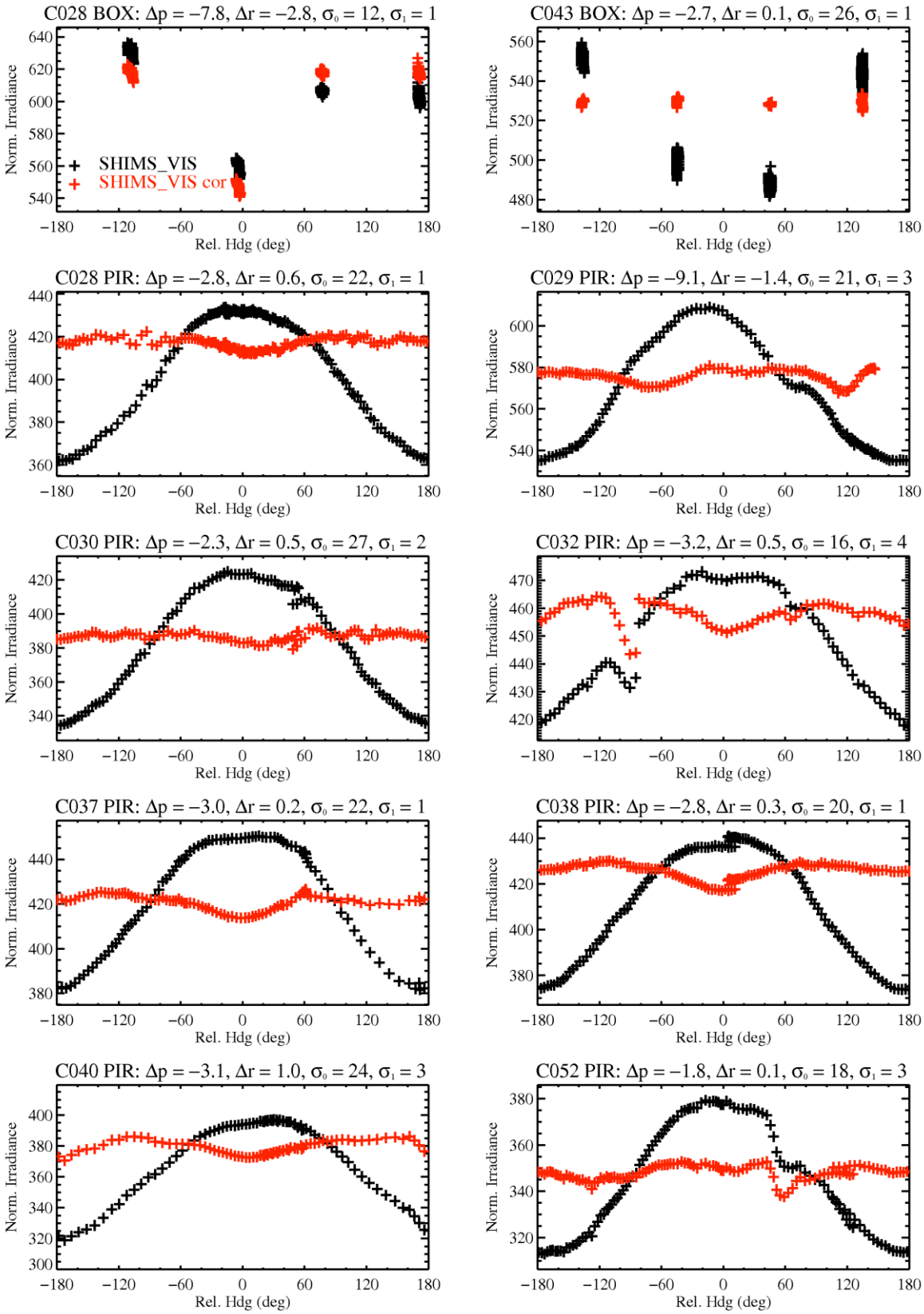

Figure 3.7: Normalised irradiances from the SHIMS visible module for manoeuvres during the CLARIFY-2017 campaign. Black indicates raw data, red indicates data corrected by optimal attitude corrections (values for ΔP and ΔR are given in the titles, as well as initial and corrected standard deviations σ_0 and σ_1)

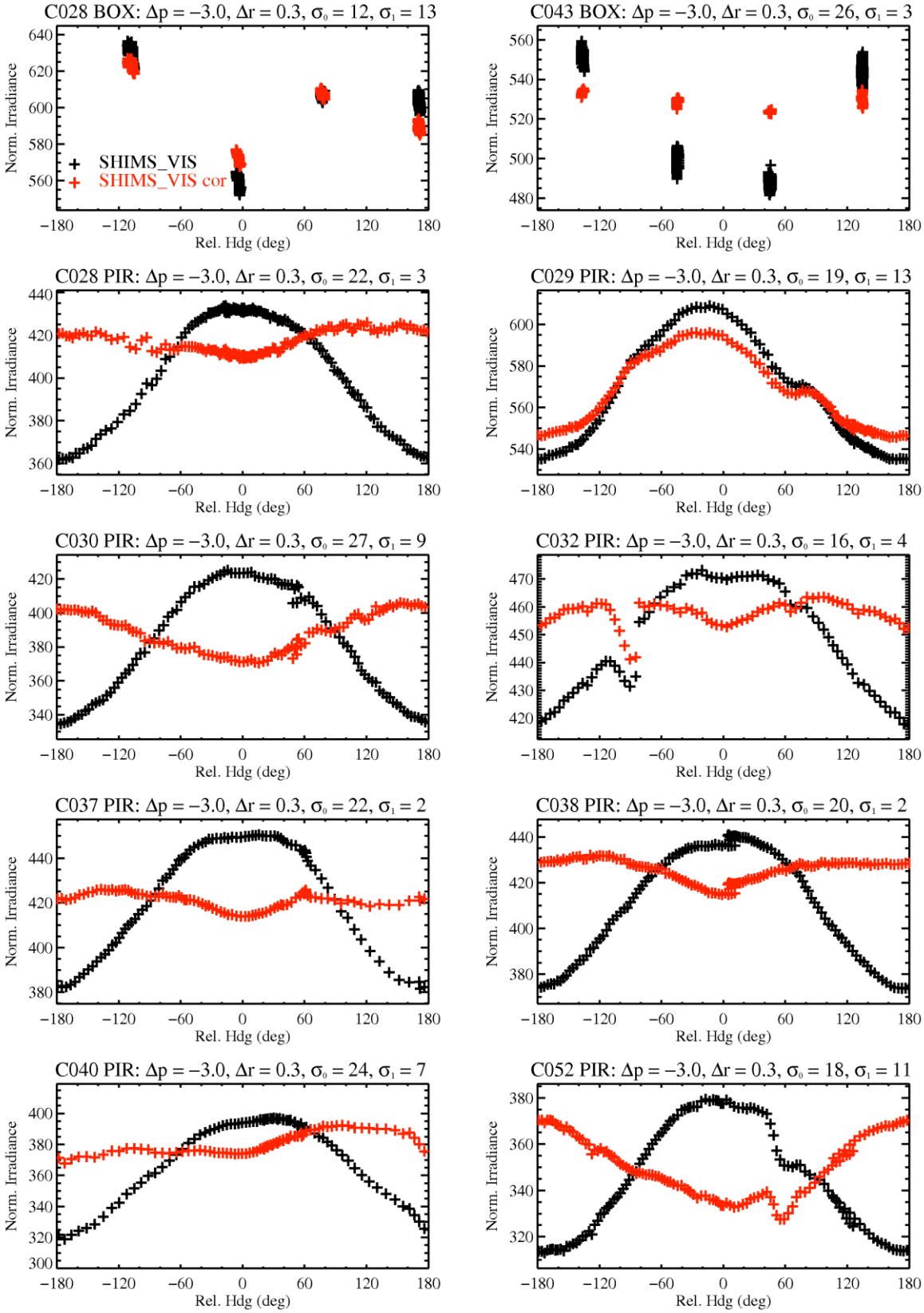

Figure 3.8: Normalised irradiances from the SHIMS visible module for manoeuvres during the CLARIFY-2017 campaign. Black indicates raw data, red indicates data corrected by optimal attitude corrections of ΔP = -3 and ΔR = +0.3 (values for the initial and corrected standard deviations σ_0 and σ_1 given in the titles)

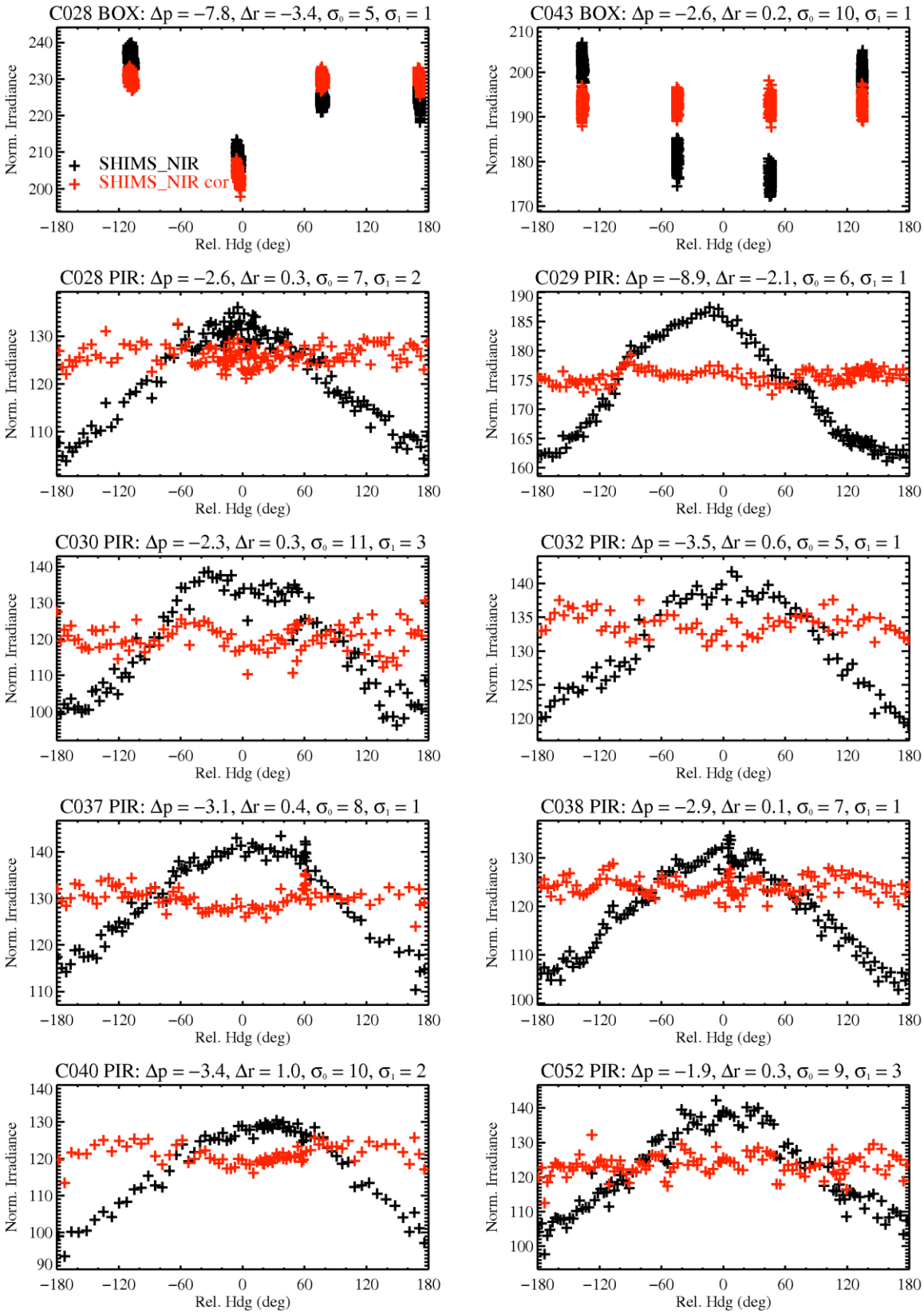

Figure 3.9: Normalised irradiances from the SHIMS near-infrared module for manoeuvres during the CLARIFY-2017 campaign. Black indicates raw data, red indicates data corrected by optimal attitude corrections (values for ΔP and ΔR are given in the titles, as well as initial and corrected standard deviations σ_0 and σ_1)

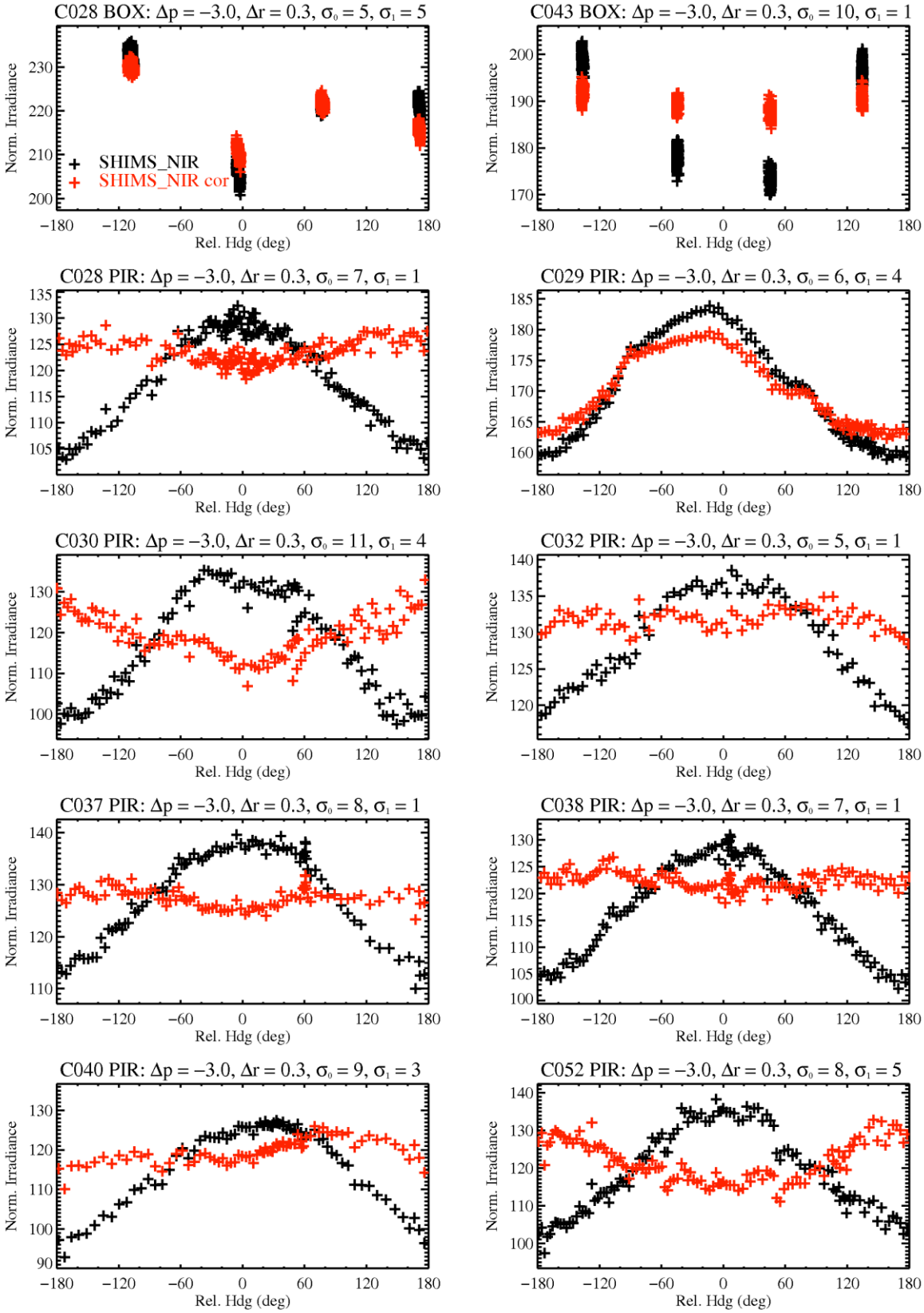

Figure 3.10: Normalised irradiances from the SHIMS near-infrared module for manoeuvres during the CLARIFY-2017 campaign. Black indicates raw data, red indicates data corrected by optimal attitude corrections of ΔP = -3 and ΔR = +0.3 (values for the initial and corrected standard deviations σ_0 and σ_1 given in the titles)

4. Correcting the CLARIFY-2017 radiation data

4.1 Applying pitch and roll corrections to whole flight data

P&R corrections have now been applied to observations from all CLARIFY-2017 flights for which data was available (C028 through C053). Data was set to missing when β (Eq. 2.1) exceeded 80°, the absolute value of the roll exceeded 7°, or the flux exceeded a maximum threshold (1380, 700, 950, and 350 Wm^{-2} for BBR clear, BBR red, SHIMS vis and SHIMS nir respectively).

Figures 4.1 and 4.2 show the results of this correction for the two flights that contained box patterns, C028 and C043. Black lines in Figs 4.1 and 4.2 show the raw data (i.e. inverted FAAM data for the BBRs) and red crosses show the P&R corrected data (v1, as described in Section 3 and above). Additionally, Figs 4.1 and 4.2 include F_{crit} values in cyan, which are used to determine whether irradiances are predominantly direct or diffuse (Eq. 2.3), and modelled irradiances for which we use a standard tropical atmospheric column and clear-sky conditions (green lines). The modelled irradiances, as a function of solar zenith angle and altitude, for wavebands corresponding to each instrument are shown in Fig. 4.3. For C028 and C043, the P&R corrections alter the irradiances by at most +/-10 % of the measurements. Most of the changes are small (<5 %) relative to the measurements. It is clear from Figs 4.1 and 4.2 that the BBR clear dome irradiances closely approximate the modelled values. The clear-sky flux measurements from the clear dome are on average 2.7 % smaller than the modelled values for the entire campaign. In contrast, the BBR red dome has corrected irradiances that 11.1 % smaller than the modelled values. This suggests that the BBR red dome instrument is significantly underestimating the near-infrared irradiances, possibly owing to imperfections on the dome from sandblasting in previous campaigns as inferred in the last section, or due to instrumental errors.

In contrast to the BBRs, the SHIMS v1 values systematically underestimate the modelled irradiances by 30-40% on average, with both the visible and near-infrared modules affected. This indicates an issue with the SHIMS instrument or with its calibration, and this disparity is relatively consistent for the entirety of the campaign and even extends to the lower instruments (not shown here). We now attempt to rectify this disparity and correct the SHIMS data using the BBR measurements.

4.2 Correcting SHIMS to the BBR values

The calibration routine for the SHIMS data uses the following equation:

$$c_d = (r_d - d) \times \left({}^{L_t}/_{F_t}\right) \times \left({}^{C_c}/_{L_s}\right) \quad (4.1)$$

Where c_d is the calibrated data, r_d is the raw data, d is the dark current, L_t is the laboratory transfer measurement, F_t is the field transfer measurement, C_c is the

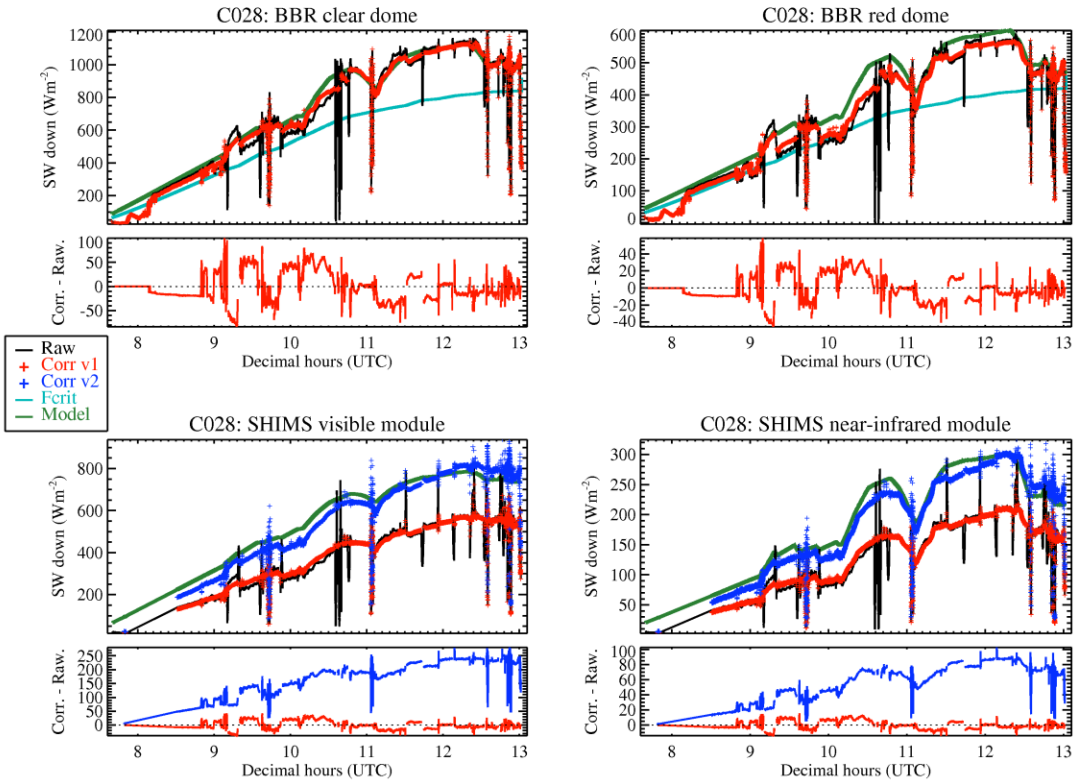

Figure 4.1: Raw downwelling SW irradiances, corrected irradiances, the critical flux threshold F_{crit} (Eq. 2.3) and modelled irradiances for flight C028

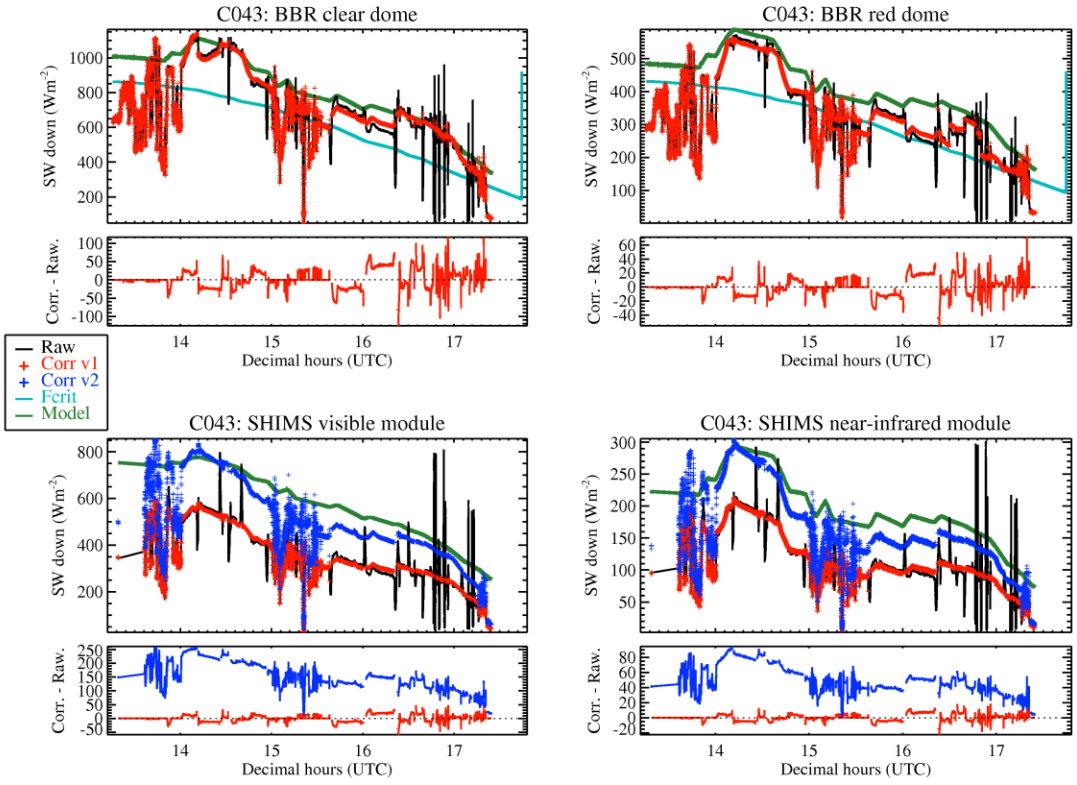

Figure 4.2: The same as Fig. 4.1 but for flight C043

calibration certificate for the local standard, and L_S is the local standard. As both the visible and near-infrared SHIMS measurements exhibit similar deviations from the modelled irradiances (30-40 %), and the dark currents are independent for the two modules, this suggests that the issue lies with constant multiplicative factor in Eq. 4.1 (i.e. components 2 and 3 on the right hand side). Thus in order to 'correct' the data to the BBR values whilst keeping the result physical (i.e. by assuming a constant error in one of the constant factors in Eq. 4.1), it is necessary to multiply all of the data by a constant factor such as the campaign-mean difference between the BBR measurements and the SHIMS measurements.

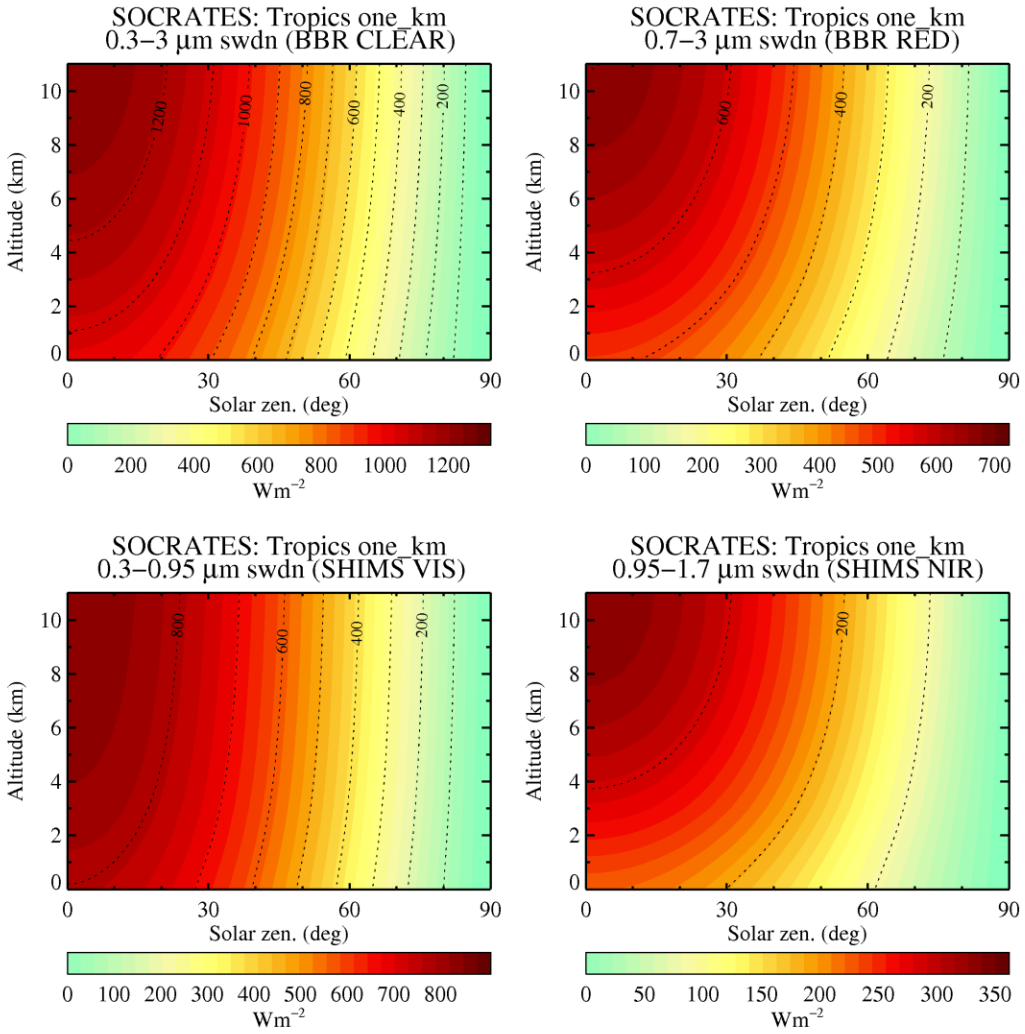

Figure 4.3: Modelled downwelling total shortwave fluxes in 4 wavebands corresponding to the various instruments as a function of solar zenith angle (x-axis) and altitude (y-axis). The model assumes clear skies and uses a standard tropical atmospheric profile [McClatchey *et al*., 1972]

The irradiance spectrum surveyed by the BBRs (0.3-3 µm) overlaps with the spectrum surveyed by the SHIMS visible module (0.3-0.95 µm). In particular, subtracting the BBR's red dome data from the clear dome data gives irradiances between the spectral range 0.3-0.7 µm that are comparable with the corresponding irradiances from the SHIMS visible module. However, owing to the poor agreement between the BBR red dome data and the modelled irradiances

(Figs 4.1 and 4.2), and due to the curious unphysical data in the pirouettes and manoeuvres, we elect not to use the BBR red dome data to correct the SHIMS measurements. Instead, we compare the BBR clear data (0.3-3 μm) with the sum of the SHIMS visible (0.3-0.95 μm) and near infrared (0.95-1.7 μm) data and a small model-derived increment for the wavelength spectrum spanning 1.7-3 μm. We define this increment (ε) as the ratio of the total downwelling shortwave flux in the wavelength spectrum 1.7-3 μm to the flux in the spectrum 0.3-1.7 μm. We calculate ε on pressure levels from the surface to 0.3 hPa and for 1.25° increments of the solar zenith angle, using SOCRATES and the clear-sky standard tropical atmospheric column. We find that the ratio ε is mostly invariant to solar zenith angle, and ranges from 5 % at the surface to 9 % at high altitudes. Thus we compare (SHIMS vis + nir) × (1+ε(z,θ)) to the BBR clear dome irradiances to derive a suitable constant correction factor for SHIMS. It is important to note that below an atmospheric aerosol layer, ε will be different compared to unpolluted conditions. To partially overcome this issue, we will only compare SHIMS and BBR data collected above 2 km altitude.

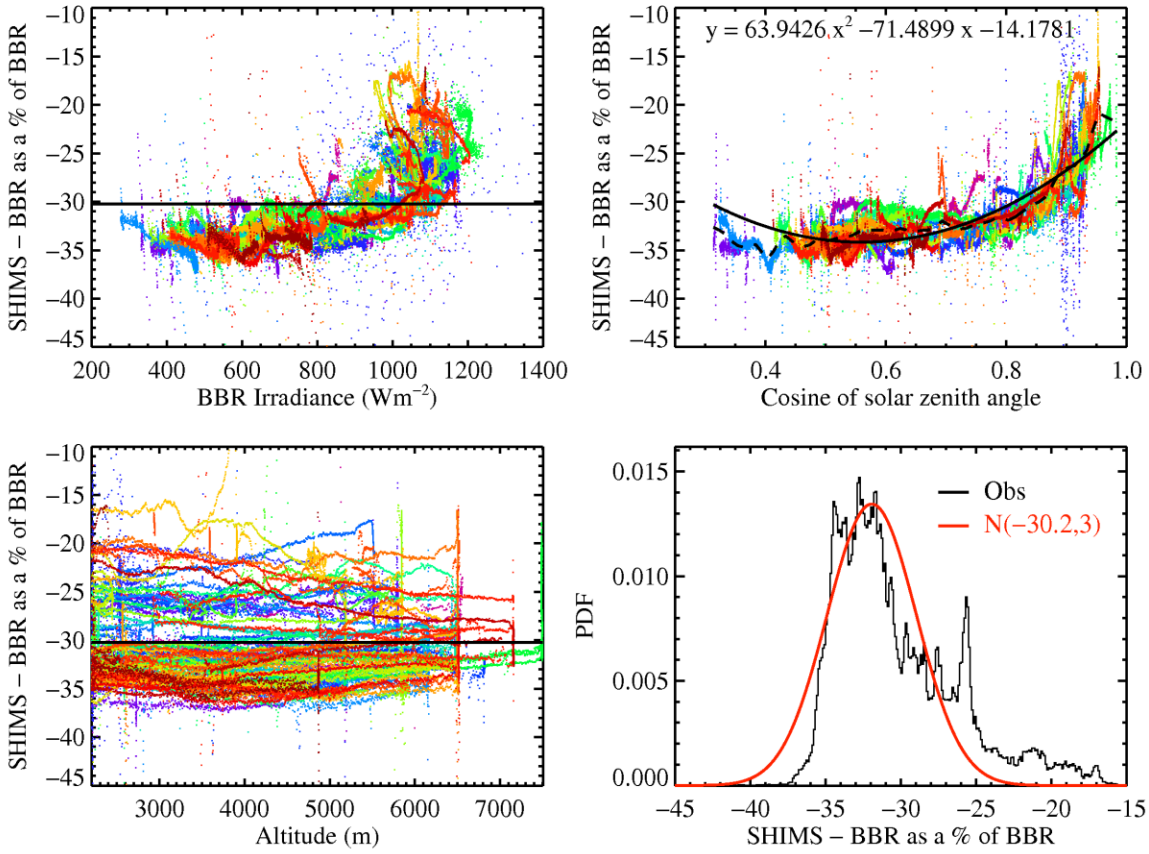

Figure 4.4: Differences between SHIMS (vis + nir + ε, 0.3-3μm) and BBR clear corrected irradiances as a percentage of the BBR clear irradiances. Each point denotes a single observation, with all observations in clear-sky conditions and at altitudes > 2 km plotted. Different colours correspond to different flights. The SHIMS-BBR differences are plotted against: (top left) BBR irradiances, (top right) cosine of the solar zenith angle, (bottom left) altitude, and (bottom right) as a PDF with a normal fit for the residuals from subtracting the polynomial in the top right plot from the data

Figure 4.4 shows the differences between SHIMS and the BBR clear dome for all high altitude (z > 2 km) data from the CLARIFY-2017 campaign. On average, the SHIMS data is 30 % smaller than the BBR data, although there is a wide spread in the percentage differences, which can be approximated (albeit imperfectly) using a normal distribution with mean (μ) = -32 % and standard deviation (σ) = 3 %. Note that the normal distribution may not be appropriate here as fitted values less than 100 % (which have small but finite probability in this distribution) would imply negative radiation data, which would be unphysical. It is also interesting to note the curved trend in (SHIMS-BBR)/BBR with the cosine of θ (Fig. 4.4). This trend closely follows a second-order polynomial, which is shown as a black line in Fig. 4.4. However, the physical reasoning for this trend is elusive, and any correction to the data should be a single factor in order to keep the data physical.

We correct the SHIMS v1 data to the BBR values using the formula: SHIMSv2 = SHIMSv1 × 1.43. By multiplying the uncertainties due to P&R/cosine corrections in the SHIMSv1 and BBR data, we derive an uncertainty in the corrected (i.e. SHIMSv2) measurements of ±**20 %** at the 2σ level. This can be compared to the < ±8 % standard deviation in the SHIMSv1 data which we also assume is wrong by a factor of 30% (hence the correction) meaning that the absolute uncertainty in the measured data (i.e. SHIMSv1) is more like 30-40 %. All of these values are extremely tentative and not particularly useful given that we are unable to provide a reason why the SHIMS v1 data is 30 % smaller than the BBR measurements, and given that the BBR measurements are subject to their own uncertainty. It will therefore be important to establish why the SHIMS data is 30 % smaller than the BBR values in order to remove this additional uncertainty. Figures 4.1 and 4.2 show the SHIMSv2 data (blue crosses), which is clearly a much closer fit to the modelled values (green lines) than the SHIMSv1 data (red crosses).

4.3 Comparing SHIMS irradiance spectra to modelled values

Figure 4.5 compares the SHIMSv2 irradiance spectra for three aircraft manoeuvres (C037 PIR, C038 PIR and C043 BOX) to the modelled values from SOCRATES. We represent biomass-burning aerosol (BBA) in the model using mass mixing ratio and optical depth forecasts from the Met Office Operational model. The total-column BBA optical depths are approximately 0.13 for C037 and C038, and 0.28 for C043. The model solves the 2-stream radiative transfer equation for 260 wavebands spanning the shortwave spectrum, and utilises a standard tropical atmospheric column profile. From Fig. 4.5, the SHIMSv2 and modelled total irradiances are very similar (agreeing to within 10 %), and the SHIMSv2 data mostly mirrors the peaks and troughs in the modelled spectra. However, there is evidently an issue in the ultraviolet spectrum where SHIMSv2 exhibits smaller values than the model, which may relate to differing ozone concentrations between the model and ambient atmospheres, or might be due to instrumental error. In addition, there is a clear disparity between the model and the observations at ~1.27 μm. We have performed sensitivity studies in which we double concentrations of primary gaseous absorbers at 1.27 μm (water vapour, oxygen and carbon dioxide), with the result that none of these species seems to be able to explain this curious signal. Keith Shine (University of Reading) suggests that the issue is due to lack of representation of O_2-O_2 continuum absorption in the SOCRATES radiation code, which is currently being

investigated by the code's owner (James Manners) and should be included in future versions of the 260wb spectral file. In summary, the differences between SHIMSv2 and the model are relatively modest, which suggests that applying a spectrally invariant correction factor to the observed SHIMS flux densities (see above) in order to rectify the disparity between SHIMS and the BBRs is appropriate.

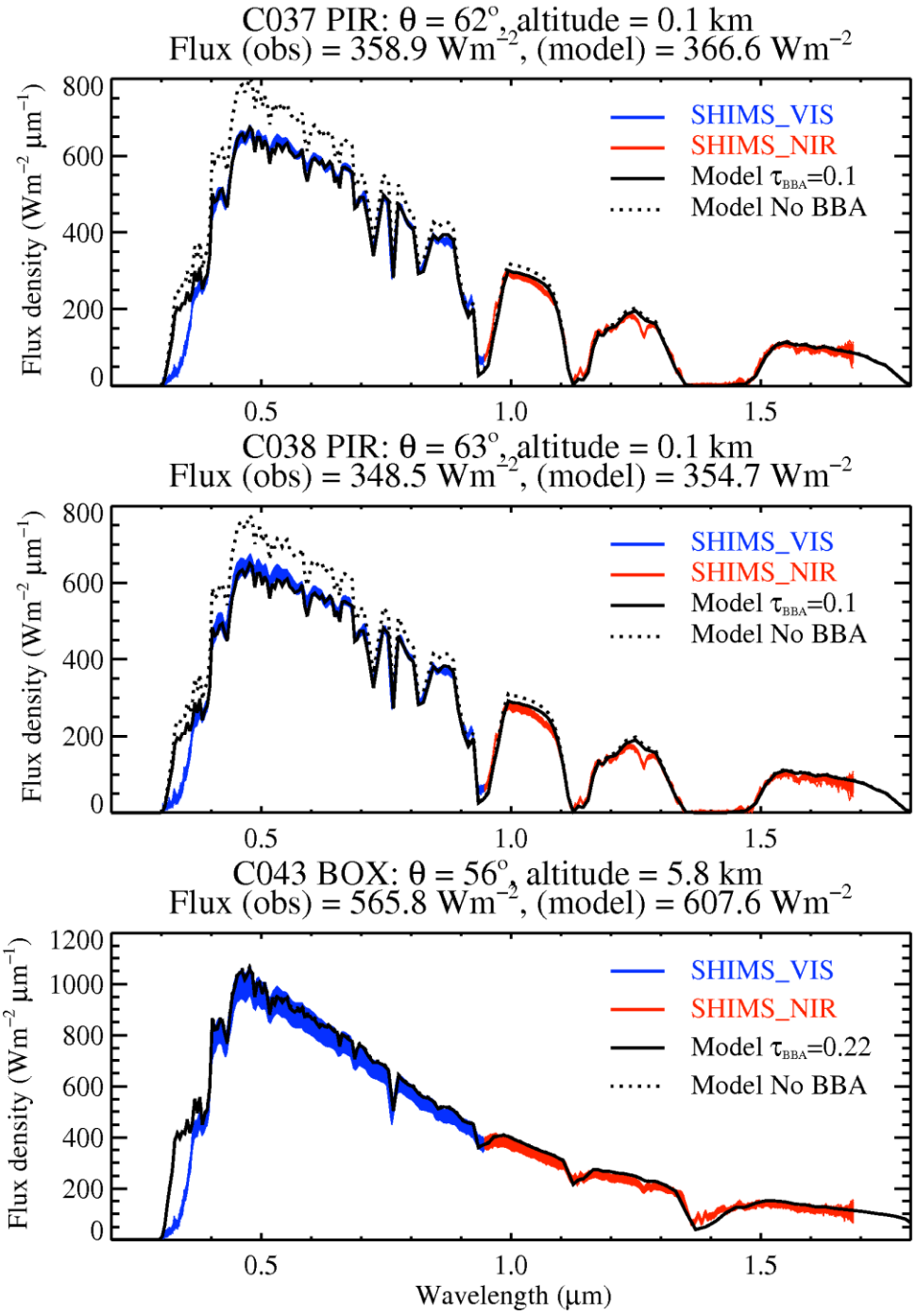

Figure 4.5: Irradiance flux densities from the SHIMS visible (blue) and near-infrared (red) modules during three CLARIFY-2017 aircraft manoeuvres, plotted against modelled values (black)

5. Summary

Pitch and roll corrections have been revisited and an algorithm documented, with P&R optimizations then applied to radiation measurements from the CLARIFY-2017 campaign. We find clear instances of unphysical data from the BBR red dome (and to a lesser extent the clear dome) during pirouette manoeuvres, but not contemporaneously for the SHIMS data. This may be due to contamination on the red and clear domes, or due to an instrument or calibration issue that needs to be examined. **The results of our study suggests that the red-dome instrument may be recording unphysical radiation measurements.**

We also find a ~30 % low bias for the SHIMS measurements when compared to both the BBRs and modelled fluxes. Although SHIMS measurements have suffered similar sized biases in previous campaigns, this issue will also need to be investigated to ensure that the instrument's calibration procedure is appropriate. Finally, pirouettes performed at small solar zenith angles exhibit large optimal pitch-offset tendencies and vice versa for pirouettes performed at large solar zenith angles. This suggests that the cosine effect factor, which was derived for the BBRs, is not entirely appropriate for either the BBR or the SHIMS instrument and needs to be re-evaluated for each instrument. When correcting the SHIMS data to the BBR values, it was found that the disparity varied non-linearly with the cosine of the solar zenith angle. This indicates that the cosine correction factor C_{eff} as determined for the BBRs is not appropriate for the SHIMS instrument, as might be expected, due to differences in its internal design. **We recommend that C_{eff} is re-determined for the BBRs (red and clear dome independently) and for SHIMS**.

From the P&R corrected irradiances taken from the pirouette and box pattern manoeuvres, we estimate uncertainty due to P&R, dirt/damage, and cosine issues of < 7 % for the BBR clear dome, < 12 % for the BBR red dome, < 7 % for the SHIMS visible module, and < 8 % for the SHIMS near-infrared module. However, this uncertainty is subject to the caveats that only two of the manoeuvres provided acceptable data for the BBR red dome, and that the SHIMS measurements are approximately 30 % smaller than the equivalent BBR measurements. When including the uncertainty from adding a correction factor (i.e. 1/1-30%), the total 2σ uncertainty due to P&R, dirt/damage, and cosine issues in the SHIMS data rises to ± 30-40 %. This highlights the importance of identifying the issue with SHIMS for future campaigns.

From the pirouettes performed after the flight (e.g. C037 and C052) there is some evidence of a 'dirty dip' in the irradiance signature at small relative headings, which arises from sandblasting or more likely aerosol contamination on the instrument covering (e.g. Fig. 3.2). This issue is not apparent in the pre-flight pirouettes (e.g. C038 and C040), and is more obvious for the BBRs than SHIMS. Also, a dirty dip appears to be present in the C028 box pattern for both SHIMS and the BBRs. As this issue primarily affects data recorded when the aircraft is facing into the sun (i.e. $-40^{o} < H_{S} < +40^{o}$), **we recommend that box patterns with four legs are performed such that no leg aims directly into the sun in order to provide usable data for P&R corrections**, for instance, at relative headings of ±45° and ±135° (Fig. 5.1). Else we recommend performing more

than four legs for each box pattern (e.g. eight legs), with legs lasting ~2 minutes rather than the customary 5 minutes, in order to better constrain the P&R offsets. 'Into the sun' runs may be useful for characterising the condition of the instrument, but are not useful for deriving P&R offsets.

Resulting from this study, we recommend the following:

1. The BBR red dome exhibits curious irradiance signatures during the pirouette manoeuvres which suggests an issue with instrument – this should be checked

2. Cosine correction factors (C_{eff}) should be calculated for both the BBR and SHIMS instruments

3. Pirouettes should only be performed during clear-sky conditions and when the sun is not too low in the sky (i.e. not when $\theta > 74^{o}$)

4. Box patterns with four legs should have no legs facing directly into the sun, instead being performed at relative headings of ±45° and ±135° (Fig. 5.1), in order to provide usable data for P&R corrections. Performing box patterns with 8 legs and shorter leg-durations (e.g. 2 mins) may be preferable to 4 legs for deriving P&R offsets

5. The SHIMS calibration routine must be checked to identify why SHIMS is consistently underestimating irradiances by ~30 % compared to the BBRs

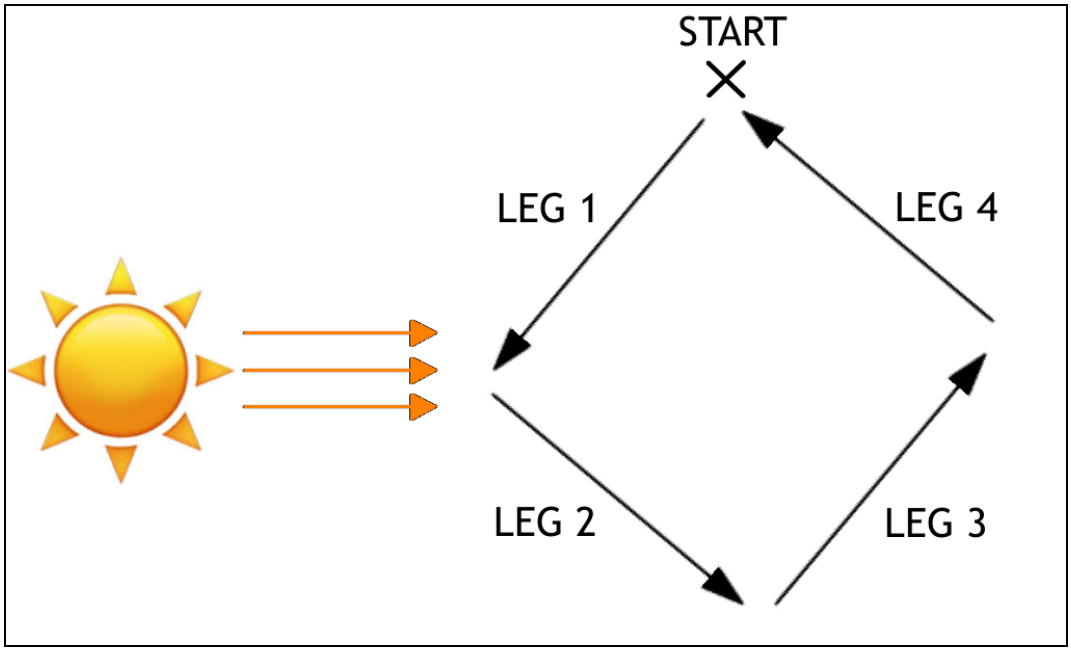

Figure 5.1: Schematic showing an optimal 4-legged box pattern which comprises relative headings of ±45° and ±135° or thereabouts

Appendix - IDL code for pitch and roll optimization

```
pro corr_flx, flx, fdir, ceff, szen, sunhdg, ptch, roll, dp, dr, fflx, flx_cor=flx_cor
1/1

d2r=!pi/180.
rollx = roll + dr          ; add the roll from GIN to the roll offset (dr)
ptchx = ptch + dp                ; add the pitch from GIN to the pitch offset (dp)

; Firstly convert angles to radians
szenrad  = szen*d2r  ; Convert solar zenith angle (szen) to radians
rollrad  = rollx*d2r
ptchrad  = ptchx*d2r
sunhdgrad = sunhdg*d2r

; Only apply the correction if roll < 7; fflx = 1 (i.e. flx > fcrit); theta < 80
flx_cor = flx
for i = 0,n_elements(szenrad)-1 do begin
  rcosth = sin(rollrad(i))*sin(szenrad(i))*sin(sunhdgrad(i)) + $
        cos(rollrad(i))*cos(ptchrad(i))*cos(szenrad(i)) - $
        cos(rollrad(i))*sin(ptchrad(i))*sin(szenrad(i))*cos(sunhdgrad(i))
  theta=acos(rcosth)/d2r
  fac=1.-fdir(i)*(1-ceff(i)*rcosth/cos(szenrad(i)))
  if (abs(roll(i)) le 7.0) and (fflx(i) eq 1) and $
    (theta le 80.) and (szen(i) gt 0.) and (szen(i) lt 90.) then begin
    flx_cor(i)=flx(i)/fac
  endif
endfor
end
```

```
pro invert_faam_corr, flx, szen, azim, hdg, roll, ptch, dr, dp, red=red, clr=clr, $      1/3
                drc=drc, dpc=dpc, flx_cor=flx_cor, ceff=ceff, fdir=fdir, fcrit=fcrit, $
                rollbar=rollbar, ptchbar=ptchbar, sunhdg=sunhdg, flag_flx=flag_flx

d2r=!pi/180.

; For roll and pitch from GIN, average over the last 2 seconds and add offsets
rollbar = run_2_avg(roll)
ptchbar = run_2_avg(ptch)
rollx = rollbar + dr
ptchx = ptchbar + dp

; Convert all angles to radians
szenrad = szen*d2r
azimrad = azim*d2r
rollrad = rollx*d2r
ptchrad = ptchx*d2r
hdgrad  = hdg*d2r
sunhdgrad = azimrad-hdgrad
sunhdg    = sunhdgrad/d2r
for i = 0,n_elements(sunhdg)-1 do if (sunhdg(i) gt 180.) then sunhdg(i) = sunhdg(i)-360.
for i = 0,n_elements(sunhdg)-1 do if (sunhdg(i) lt -180.) then sunhdg(i) = sunhdg(i)+360.
```

```
; Calculate FAAM values for the cosine effect and FDIR (just 0.95)                    2/3
ceff_f = [1.010, 1.005, 1.005, 1.005, 1.000, 0.995, 0.985, 0.970, 0.930, 0.930]
fdir_f = [0.950, 0.950, 0.950, 0.950, 0.950, 0.950, 0.950, 0.950, 0.950, 0.950]

ceff = fltarr(n_elements(szen)) & ceff(*)=!values.f_nan
fdir = fltarr(n_elements(szen)) & fdir(*)=!values.f_nan
for i = 0,n_elements(szen)-1 do begin
  if (finite(szen(i)) eq 1) then begin
    ceff(i)=ceff_f(min([round(szen(i)/10),9]))
    fdir(i)=fdir_f(min([round(szen(i)/10),9]))
  endif
endfor

; Calculate critical flux values using the solar zenith angle
fcrit = fltarr(n_elements(szenrad)) & fcrit(*)=!values.f_nan
for i = 0,n_elements(szenrad)-1 do begin
  if (finite(szenrad(i)) eq 1) then begin
    fcrit(i)=920.*(cos(szenrad(i))^1.28)
  endif
endfor

; Calculate rtheta and theta values – Eqs 1 and 2
rcosth = fltarr(n_elements(szenrad)) & rcosth(*)=!values.f_nan
theta  = fltarr(n_elements(szenrad)) & theta(*)=!values.f_nan
fac    = fltarr(n_elements(szenrad)) & fac(*)=!values.f_nan
for i = 0,n_elements(szenrad)-1 do begin
  if (finite(szenrad(i)) eq 1) and (finite(rollrad(i)) eq 1) and $
    (finite(ptchrad(i)) eq 1) and (finite(sunhdgrad(i)) eq 1) then begin
    rcosth(i) = sin(rollrad(i))*sin(szenrad(i))*sin(sunhdgrad(i)) + $
                cos(rollrad(i))*cos(ptchrad(i))*cos(szenrad(i)) - $
                cos(rollrad(i))*sin(ptchrad(i))*sin(szenrad(i))*cos(sunhdgrad(i))
    theta(i)=acos(rcosth(i))/d2r
    fac(i)=1.-fdir(i)*(1-ceff(i)*rcosth(i)/cos(szenrad(i)))
  endif else begin
    fac(i)=!values.f_nan
  endelse
endfor
; If red dome (i.e. red=1) then use the roll and pitch coefficients
; for the clear dome to calculate rtheta and theta values
if (keyword_set(red) eq 1) then begin
  rcosth2  = fltarr(n_elements(szenrad)) & rcosth2(*)=!values.f_nan
  theta2   = fltarr(n_elements(szenrad)) & theta2(*)=!values.f_nan
  fac2     = fltarr(n_elements(szenrad)) & fac2(*)=!values.f_nan
  rollrad2 = (rollbar+drc)*d2r
  ptchrad2 = (ptchbar+drc)*d2r
  for i = 0,n_elements(szenrad)-1 do begin
   if (finite(szenrad(i)) eq 1) and (finite(rollrad(i)) eq 1) and $
      (finite(ptchrad(i)) eq 1) and (finite(sunhdgrad(i)) eq 1) then begin
      rcosth2(i) = sin(rollrad2(i))*sin(szenrad(i))*sin(sunhdgrad(i)) + $
                   cos(rollrad2(i))*cos(ptchrad2(i))*cos(szenrad(i)) - $
                   cos(rollrad2(i))*sin(ptchrad2(i))*sin(szenrad(i))*cos(sunhdgrad(i))
      theta2(i)=acos(rcosth2(i))/d2r
      fac2(i)=1.-fdir(i)*(1-ceff(i)*rcosth2(i)/cos(szenrad(i)))
    endif else begin
      fac2(i)=!values.f_nan
    endelse
  endfor
endif
```

3/3

```
; Finally invert the fluxes - only invert flux if the following conditions
; are met:
; 1 - roll angle from GIN within +/- 7o
; 2 - the inverted flux is greater or equal to a critical value
; 3 - the sun is high enough (i.e. beta le 80o)
; 4 - solar zenith angle is between 0. and 90.
; 5 - corrected flx
; 6 - data is available for solar szen, roll, ptch, and sunheading
if (keyword_set(red) eq 1) then begin
  flx_cor = flx
  clr_cor = clr
  flag_flx = intarr(n_elements(flx))
  for i = 0,n_elements(szenrad)-1 do begin
    if (abs(rollbar(i)) le 7.0) and (clr(i)*fac2(i) ge fcrit(i)) and $
      (theta2(i) le 80.) and (szen(i) gt 0.) and (szen(i) lt 90.) and $
      (finite(fac2(i)) eq 1) then begin
      flx_cor(i)=flx(i)*fac(i)
      clr_cor(i)=clr(i)*fac2(i)
    endif
    if (clr_cor(i) ge fcrit(i)) and (finite(clr_cor(i)) eq 1) then flag_flx(i)=1
  endfor
endif else begin
  flx_cor = flx
  flag_flx = intarr(n_elements(flx))
  for i = 0,n_elements(szenrad)-1 do begin
    if (abs(rollbar(i)) le 7.0) and (flx(i)*fac(i) ge fcrit(i)) and $
      (theta(i) le 80.) and (szen(i) gt 0.) and (szen(i) lt 90.) and $
      (finite(fac(i)) eq 1) then begin
      flx_cor(i)=flx(i)*fac(i)
    endif
    if (flx_cor(i) ge fcrit(i)) and (finite(flx_cor(i)) eq 1) then flag_flx(i)=1
  endfor
endelse
; For sake of completion, multiply the output fcrit by half if red dome
if (keyword_set(red) eq 1) then fcrit=fcrit*0.5
```

References

Bannehr, L., and R. Schwiesow (1992), A technique to account for the misalignment of pyranometers installed on aircraft, *J. Atmos. Ocean. Tech.*, 10, 774-777

Boers, R., M. Mitchell, P. B. Krummel (1998), Correction of aircraft pyranometer measurements for diffuse radiance and alignment errors, *J. Geophys. Res*, 103, D13, 16,753-16,758

Cluley, A. P., and J. P. Cowley (1980), An aircraft-mounted pyranometer, *The Meteorolical Magazine*, Met Office, No. 1297, August 1980, Vol. 109

Edwards, J. M., and A. Slingo (1996), Studies with a flexible new radiation code. I: Choosing a configuration for a large-scale model, *Q. J. R. Meteorol. Soc.*, 122, pp. 689-719. doi:10.1002/qj.49712253107

Haywood, J. M., B. T. Johnson, S. R. Osborne, J. Mulcahy, M. E. Brooks, M. A. J. Harrison, S. F. Milton, and H. E. Brindley (2011), Observations and modelling of the solar and terrestrial radiative effects of Saharan dust: a radiative closure case-study over ocean during the GERBILS campaign, *Q. J. R. Meteorol. Soc.*, 137, 1211-1226

Jones, A. C. (2017), Investigating the climatic impacts of stratospheric aerosol injection, PhD dissertation, University of Exeter, Exeter (available at http://hdl.handle.net/10871/27786)

McClatchey, R. A., *et al.* (1972), Optical Properties of the Atmosphere (Third Edition), AFCRL 72-0497, AD 753075

MRF Internal Note 4, Cluley, A. P. (1978), *The installation of an upward-facing pyranometer on MRF Hercules XV 208*, Meterological Research Unit, Royal Aircraft Establishment, Farnborough, Hampshire, U. K.

MRF Internal Note 31, Foot, J. S., P. Hignett, C. G. Kilsby (1986), *Investigation into errors associated with upward-facing pyranometers fitted to the MRF Hercules*, Meterological Research Unit, RAF Cardington, Bedfordshire, U. K.

MRF Internal Note 56, Saunders, R. W., and J. A. Barnes (1991), *Intercomparison flights of pyranometers and pyrgeometers on the MRF C-130*, Meteorological Research Flight, R.A.E., Farnborough, Hampshire

MRF Technical Note 5, Saunders, R. W., J. S. Foot, C. G. Kilsby, and J. H. Seymour (1991), *Report of Broad-Band Radiative Fluxes Working Group*, Meteorological Research Flight, R.A.E., Farnborough, Hampshire

MRF Technical Note 8, J. H. Seymour (1992), Pyranometer Calibrations at Ascension Island, Meteorological Research Flight, Defence Research Agency, Farnborough, Hampshire

OBR Technical Note 90, A. K. Vance, J. Norwood-Brown, and D. O'Sullivan (2017), SWS-SHIMS Calibration and Uncertainties, Met Office, Exeter, UK

Ryder, C. L., E. J. Highwood, T. M. Lai, H. Sodemann, and J. H. Marsham (2013), Impact of atmospheric transport on the evolution of microphysical and optical properties of Saharan dust, *Geophys. Res. Lett.*, 40, 2433–2438, doi:10.1002/grl.50482.

Saunders, R. W., G. Brogniez, J. C. Buriez, R. Meerkötter, and P. Wendling (1992), A Comparison of Measured and Modeled Broadband Fluxes from Aircraft Data during the ICE '89 Field Experiment, *J. Atmos. Ocean. Tech.*, 9, 391–406
Schmetz, J. and M. Beniston (1986), Relative effects of solar and infrared radiative forcing in a mesoscale model, *Boundary Layer Meteorol.*, 34, 137-155.

Met Office
FitzRoy Road, Exeter
Devon EX1 3PB
United Kingdom

Tel: 0870 900 0100
Fax: 0870 900 5050
enquiries@metoffice.gov.uk
www.metoffice.gov.uk